Author's Accepted Manuscript

www.elsevier.com/locate/dsr2

Climate change projection for the western tropical Pacific Ocean using a high-resolution ocean model: Implications for tuna fisheries

R.J. Matear, M.A. Chamberlain, C. Sun, M. Feng

PII: S0967-0645(14)00175-1
DOI: http://dx.doi.org/10.1016/j.dsr2.2014.07.003
Reference: DSRII3674

To appear in: *Deep-Sea Research II*

Climate change projection for the western tropical Pacific Ocean using a high-resolution ocean model: implications for tuna fisheries

R. J. Matear[a], M. A. Chamberlain[a], C. Sun[b], M. Feng[b]

[a] *Centre for Australian Weather and Climate Research (CAWCR), a partnership between CSIRO and the Bureau of Meteorology; CSIRO Marine and Atmospheric Research, CSIRO Marine Laboratories, GPO Box 1538, Hobart, Tasmania, Australia*

[b] *CSIRO Marine and Atmospheric Research, CSIRO Marine Laboratories, Perth, Western Australia, Australia*

Abstract

The Western Pacific Warm Pool is a region of high tuna catch, and how future climate change might impact the tuna fisheries is an important regional issue. By using a high-resolution ocean model forced by the simulated climate of the 2060s, we investigate whether enhanced spatial resolution and bias correction of the mean state could alter the climate change projection for the western tropical Pacific and examine the consequences this might have for tropical tuna distributions.

For most of the physical environmental variables, enhanced resolution and bias correction had only a minor impact on the projected changes. The climate projections showed a maximum surface warming east of the Warm Pool, a shoaling of the thermocline in the Warm Pool, and an eastward expansion of the Warm Pool. In the Warm Pool, the shoaling of the thermocline raises the nutricline into the photic zone and increases phytoplankton and primary productivity, a feature that is most evident in the high-resolution model projection but also weakly present in the coarse-resolution projection.

The phytoplankton and primary productivity response to climate change was where ocean model resolution produced a clear difference. With enhanced resolution, the simulation had stronger and better-defined zonal currents, which were more consistent with observations. Along the equator, the high-resolution model enabled vertical current shear mixing to generate

Email address: richard.matear@csiro.au (R. J. Matear)

a sub-surface phytoplankton maximum both inside and outside the Warm Pool, which is an observed phenomenon. With climate change, the enhanced-resolution model projected enhanced vertical shear mixing, increased vertical supply of nutrients to the photic zone, and increased sub-surface phytoplankton concentrations. The increase in sub-surface phytoplankton concentrations helps to offset the decline in surface phytoplankton concentrations and results in a projection of almost no change in the western tropical Pacific primary productivity. In contrast, the low-resolution model projected a substantial reduction in phytoplankton concentrations and primary productivity; such a response is typical of climate change projections for the region. Importantly, enhanced resolution dramatically altered the projected response of phytoplankton and primary productivity to climate change. Using the enhanced-resolution model, the projected increase in the Warm Pool with little change in primary productivity and in suitable habitat for skipjack tuna suggest that by the 2060s climate change will not have a large impact on skipjack tuna fisheries.

Keywords: climate change, western equatorial Pacific, primary productivity, tuna

---

1. Introduction

The upper waters of the equatorial Pacific Ocean are divided into two regions, which have distinct physical, biogeochemical and ecosystem characteristics. In the central and eastern Pacific, there is an equatorial upwelling system with relatively cold, salty, macronutrient-rich water, where primary production is iron-limited (Christian et al., 2002). In the western tropical Pacific, the water is warm, fresh and oligotrophic, and encompasses a prominent oceanographic region called the Western Pacific Warm Pool (Le Borgne et al., 2002). The Warm Pool has some of the warmest surface water in the ocean (McClain et al., 1999), and this warm water is fundamental to the large-scale deep atmospheric convection in the western Pacific region, the circulation and stratification of the upper ocean, and El Niño Southern Oscillation (ENSO) variability (Maes et al., 2010).

The zonal movement of the eastern edge of the Warm Pool appears to be important for the onset of the ENSO phases (Picaut et al., 1996), with the eastern edge moving westward during La Niñas and eastward during El Niños (Maes, 2008; Bosc et al., 2009; Maes et al., 2010). The location of the Warm Pool's eastern edge also seems to modulate the distribution of tuna in the equatorial Pacific (Lehodey et al., 2011). For example, the skipjack tuna catch appears to move with the large zonal displacement in the Warm Pool that occurs during ENSO events (Lehodey et al., 2011). Tuna fisheries contribute significantly to the livelihoods and economies of many Pacific Island Countries and Territories (Bell et al., 2013), so the way in which future climate change might impact tuna populations is a critical issue for this region.

Under the influence of climate change, the mean climate of the western tropical Pacific will probably undergo significant changes, with potentially important consequences for ENSO variability (Collins et al., 2010) and for tuna distributions (Lehodey et al., 2011). Coupled global circulation models (CGCMs) have common spatial biases in the western tropical Pacific, such as a Warm Pool eastern edge that is too far west (Brown et al., 2013a), which can potentially affect their future climate projections for the tropical Pacific (Brown et al., 2013b). To investigate the impact of climate change on the western tropical Pacific, we use simulations from a high-resolution ocean model (HOM) that gives a good representation of the present-day western tropical Pacific ocean state to make a climate projection for the 2060s (Chamberlain et al., 2012). The simulations are configured to determine the change in the mean ocean state. They also include the lower levels of the food web (i.e. phytoplankton and zooplankton). A previous study used the same simulations to predict future climate change in the Western Boundary Current region of the Southwest Pacific (Matear et al., 2013); the study showed that by resolving mesoscale features (e.g. the East Australian Current and its eddies), the oligotrophic water of the Tasman Sea is projected to have increased primary productivity, because of increased eddy activity. By comparing our climate projections with previously generated CGCM projections (e.g. Ganachaud et al., 2013), we investigate whether climate projections of the ocean state will be modified by a less-biased ocean state with enhanced model resolution. For this study, we focus on the western tropical Pacific because of its importance for tuna. In particular, we are interested in whether enhanced resolution can significantly alter the projection of primary productivity and suitable thermal habitat for skipjack tuna.

The paper is structured as follows. First, we briefly discuss the key oceanic features of the western tropical Pacific in § 2. Then, in § 3 we summarize how the future climate change projections are performed with our HOM. In § 4 we present results of the HOM simulation of the present-day ocean state and compare them with observational data and with the low-resolution model that we used to produce the climate change projection. Next, we describe in § 5 the climate change projection for the 2060s and compare our simulated projections from the high- and low-resolution models. This section also includes a comparison of the projected changes with previous results, discussion of the implications of our projected changes for tuna distributions in the western tropical Pacific, and remarks on the robustness of the projections. Finally, in § 6, we present a short summary of the limitations of our modelling approach and discuss the direction of our future work.

2. Oceanography of the Western Pacific Warm Pool

The Western Pacific Warm Pool has warm surface water, with a shallow mixed layer (at 30–40 m depth) separated from the thermocline (deeper than 65 m) by a high-salinity-gradient barrier layer (Lukas and Lindstrom, 1991). In the Warm Pool, the phytoplankton are macronutrient-limited, and a deep chlorophyll maximum occurs below the mixed layer (Barber and Chavez, 1991), where most of the primary productivity occurs (Le Borgne et al., 2011). Surface-nutrient depletion in the Warm Pool reflects the lack of upwelling and a deep thermocline, which under average climatic conditions is located near the lower limit (approximately 80 m) at which there is sufficient light for phytoplankton growth (Le Borgne et al., 2011). In addition to the large horizontal movement of the eastern edge of the Warm Pool with ENSO, the vertical structure within the Warm Pool also changes with ENSO phases. During an El Niño, the thermocline can shoal to 40 m, which raises macronutrients into the photic zone and increases primary productivity (Le Borgne et al., 2011).

The tuna fisheries of the tropical Pacific Ocean mostly consist of skipjack (*Katsuwonus pelamis*), yellowfin (*Thunnus albacares*), bigeye (*T. obesus*) and albacore (*T. alalunga*) (Lehodey et al., 2011). In 2009, catches from the western Pacific represented around 60% of the global tuna catch, of which about 70% comprises skipjack (Lehodey et al., 2013). Skipjack are found throughout the equatorial and subtropical Pacific, but catches are highest in the Warm Pool (Lehodey et al., 1997). Sustaining benefits from the tuna resources is a challenge for the Pacific Island Countries and Territories, as the quantity and distribution of the fish catch display large variability from year to year (Lehodey et al., 1997), and a changing ocean (e.g. Durack et al.,

2012) will make it even more difficult to maintain catch levels (Bell et al., 2013).

3. Methods

The climate model used in this study is the CSIRO Mk3.5 model of Rotstayn et al. (2010), hereafter referred to as CSIRO35. The CSIRO35 projection of the SRES (Special Report on Emissions Scenarios) A1B scenario (Nakicenovic et al., 2000) for the decade of the 2060s is used to force an HOM (Chamberlain et al., 2012). The selected SRES scenario describes a future world of very rapid economic growth, with a global population peaking in the middle of the century and declining thereafter, and where from mid-century there is also rapid introduction of new and more efficient technologies balanced across fossil and non-fossil energy sources (Nakicenovic et al., 2000). The HOM used in this study is the Ocean Forecasting Australia Model (Brassington et al., 2007; Oke et al., 2008), which is a near-global model (covering latitudes of 70°S to 70°N). The HOM has 47 vertical levels, with 10 m resolution in the upper 200 m, while the horizontal grid is variable: eddy-resolving around Australia (with 0.1° resolution between 90°E and 180°E and between 20°N and 70°S) and increasing to a maximum of 2° in the north Atlantic. The HOM also has a simple ocean biogeochemical formulation, namely the Whole Ocean Model with Biogeochemistry And Trophic-dynamics (WOMBAT). WOMBAT is based on Kidston et al. (2011) and has been implemented in the 3D ocean model 'Modular Ocean Model version 4' (Dietze et al., 2009); details of WOMBAT are given in Matear et al. (2013).

The HOM simulations used in this study are briefly summarised below, and Chamberlain et al. (2012) provides a detailed explanation of how the CSIRO35 climate change projection was used to simulate future climate change in the HOM.

To prepare the HOM, an initial spin-up of the ocean physics was performed, where the model was initialised with observed climatological fields (Chamberlain et al., 2012) and forced by atmospheric reanalysis products (i.e. windstresses, heat and freshwater fluxes) from 1991 to 2004 (ERA-40, Uppala et al., 2005), while the surface layer was relaxed to the observed surface temperatures (Reynolds and Smith, 1994) and salinities (Levitus, 2001) on a 30-day time-scale. HOM was then run for a second loop of atmospheric forcings in the same manner as the original spin-up for the period 1991–1994 but with WOMBAT activated. The ocean state at the end of this spin-up period was used as the initial state for the HOM present-day simulation. From the HOM spin-up, the windstresses and the heat and freshwater fluxes from the years 1993–2001 were averaged to produce a monthly climatology. To these monthly climatologies we added diurnal variability in the atmospheric forcing fields, which was obtained from the difference between the 1995 fields and the corresponding monthly climatology computed for 1995. The year 1995 was chosen because it was a moderate year, with none of the major climate indices (North Atlantic Oscillation, Antarctic Oscillation, North Pacific Oscillation and ENSO) at an extreme (Large and Yeager, 2004). High-frequency forcing can be important to the mixed-layer depth evolution (Large and Yeager, 2004), so we wanted to retain it in the forcing fields. The combined monthly climatologies with diurnal variability gave the present-day atmospheric forcing fields used to force the HOM present-day simulation. With these atmospheric forcing fields, the HOM present-day simulation was run for 10 years, and we present results from the last five years of this simulation. Analysis of the HOM simulations showed that after five years the simulations were stable (Chamberlain et al., 2012). Longer HOM simulations of just the physical system (Sun et al., 2012) revealed no decadal trend to the simulated climate change, justifying the use of a shorter simulation period to investigate the impact of climate change on phytoplankton.

For the HOM future climate change projection, we added to the present-day fields the changes in ocean state and changes in atmospheric forcings from the CSIRO35 simulation to obtain the initial ocean state and atmospheric forcing fields for the HOM future simulation. From the CSIRO35 simulation, we compute the change in atmospheric forcing and ocean state as the difference between the results of the 2060s and 1990s (i.e. 2060s state minus 1990s state). WOMBAT was incorporated into the CSIRO35 simulation to allow us to compare the simulated phytoplankton change resulting from the two models. With the future forcing fields, the HOM simulation was run for 10 years and the averaged results over the last five years of the simulation are reported here.

To investigate the impact of atmospheric changes over two decades (the 1990s and 2060s), the HOM simulations were performed as ocean forced simulations with atmospheric forcings that remove interannual variability by averaging a decade of atmospheric fields. Therefore, an important dynamical process of the western tropical Pacific, ENSO variability, is not represented in the projection and hence the simulations do not provide information on how the character of ENSO might change with climate change. What the projections do provide is information on how the mean ocean state may change with climate change.

To explore ocean–atmosphere coupling, we run an additional HOM simulation, where the 2060s winds are modified to assess how the future ocean warming pattern in the HOM could alter the atmospheric circulation and how this might affect future ocean dynamics (Chamberlain et al., 2012). To modify the winds, an atmospheric model is driven by the projected sea surface temperatures from the 2060s HOM simulation and the 2060s CGCM simulation (Chamberlain et al., 2012). These atmospheric-only simulations allow us to quantify how changes in the future ocean warming pattern between the HOM and CSIRO35 simulations alter the atmospheric circulation. The difference in the winds from these two atmospheric simulations are then added to the winds used to force the 2060s HOM simulation (called the wind-stress feedback) to investigate the potential interaction between the ocean and atmosphere in the future climate change projection of the ocean state.

4. Present-Day Simulation

Before describing the projected changes in the western tropical Pacific with climate change, we present an initial assessment of the present-day HOM simulation and compare its results with both the observed fields and the fields simulated by CSIRO35. The key features included in this assessment are the sea surface temperature (SST), sea surface salinity (SSS), mixed-layer depth (MLD), zonal flows, ocean properties along the equator, and chlorophyll *a* (Chla) concentrations.

4.1. Sea Surface Temperature, Salinity and Mixed-Layer Depth

To assess the simulated SST in the 1990s, we compare the annual mean SST pattern generated by the HOM with the observed climatological field from Reynolds and Smith (1994) (see Figure 1a,b). In the western tropical Pacific, the annual mean SST pattern is reproduced by the HOM, with $r = 0.93$ and a root mean square (RMS) temperature difference of 0.4°C. The model captures the observed east–west gradients in SST along the equator (3 ± 0.5°C/70 degrees from the simulation versus an observed gradient of 2.5 ± 0.5°C/70 degrees) but tends to underestimate the temperature by 1°C north of 5°N. The simulated extent of the Warm Pool, using the dynamic Warm Pool edge definition of Brown et al. (2013b) (i.e. the isotherm where the salinity gradient along the equator is maximal), was 29.5°C, in good agreement with the observed Warm Pool extent given by the 29.2°C isotherm (Maes et al., 2010) (compare Figure 1a,b). According to the dynamic Warm Pool edge definition (Brown et al., 2013b), the edge of the Warm Pool at the equator in the HOM 1990s simulation was located around 170°E, compared to an observed location of 165–170°E (Maes et al., 2010).

For the 1990s, the CSIRO35 simulation gives a much warmer western tropical Pacific (Figure 1c) and, using the dynamic Warm Pool edge definition, the 29.7°C isotherm defines the extent of the Warm Pool, which at the equator places the edge at about 160°E, slightly west of the observed edge at 165–170°E. For comparison with the HOM simulation, the CSIRO35 simulated SST correlation with the observations was similar (r=0.9) but the RMS temperature difference was much greater (0.9°C). Along the equator in the eastern equatorial Pacific, CSIRO35 displays a cold tongue bias, with surface water several degrees colder than the observations (Figure 1a,c); this is a common feature of many global climate models. Off the equator, CSIRO35 yields a much more extensive Warm Pool than the observations.

For the 1990s, the HOM-simulated annual mean SSS field shows good agreement with the observed climatological field from the 2009 CSIRO Atlas of Regional Seas (CARS2009; this is an updated dataset that uses the same methodology as Dunn and Ridgway (2002) and Ridgway et al. (2002) but includes more recent data; it is available at www.cmar.csiro.au/cars), with $r = 0.92$ and a RMS difference of 0.18 practical salinity units (Figure 2a,b). In comparison, the CSIRO35 1990s surface salinity has a large fresh bias (RMS difference of 1.3 practical salinity units) and a poor correlation with the observations (r=0.3) (Figure 2c).

The MLD controls the exchange of heat between the atmosphere and the ocean, as well as the light environment of the upper ocean, which affects phytoplankton growth (Ryan et al., 2002). To assess the HOM 1990s simulation, we compare the simulated monthly mean MLD with the observed mean value from CARS2009. For the CARS2009 dataset, the MLD is defined as the minimum depth at which the temperature is 0.4°C less than the value at 10 m and the salinity is 0.03 greater than the value at 10 m (Condie and Dunn, 2006); we use the same definition to compute the MLD in our model simulations. This definition of the MLD eliminates the possibility of density-compensating temperature and salinity gradients being interpreted as a well-mixed layer (Condie and Dunn, 2006). The spatial variability in the HOM-simulated 1990s MLDs is consistent with observations. The Warm

Pool has the shallowest MLDs (less than 40 m), and the HOM simulations gave MLDs about 10 m shallower than the observations (Figure 3a,b). To the east of the Warm Pool, the HOM-simulated MLDs vary between 50 m and 100 m, which is consistent with the observations. The exception occurs just north of the equator, where the simulated MLDs are slightly greater (20 m) than observed. The CSIRO35-simulated MLDs in the 1990s are generally too shallow (Figure 3c), particularly in the Warm Pool region, where the simulated MLD is only 20 m.

4.2. Temperature and Salinity Along the Equator

Along the equator, the observations from CARS2009 show a strong zonal gradient, with the warmest and freshest water found on the western side of the section (Figure 4). In the west, the isotherms shoal, and a sub-surface salinity maximum develops between 100 m and 200 m. In the HOM 1990s simulation, the equatorial temperature and salinity sections (Figures 5a and 6a) display the same features as evident in the observations: the simulation captures the magnitude of the zonal temperature and salinity gradients and exhibits a sub-surface salinity maximum on the western side of the section at the correct depth. The CSIRO35 1990s simulation also displays strong zonal temperature and salinity gradients along the equator (Figures 5c and 6c). However, the zonal temperature gradient is much greater than observed while the salinity is much lower than observed. The CSIRO35 simulation displays a sub-surface salinity maximum on the west side of the section, but it is about 30 m shallower than that in the observations.

4.3. Zonal Flow

As described by Kessler et al. (2003), the western equatorial region has an alternating pattern of upper ocean zonal currents, and both the HOM and the CSIRO35 simulations show this behaviour (Figure 7). Around the equator at about 3°N and 3°S, broad surface currents transport water westward; this South Equatorial Current (SEC) is present in the HOM simulation but has more north–south structure than in the CSIRO35 simulation (Figure 7a,c). Beneath the atmospheric convergence zones on both sides of the equator, eastward flowing currents appear near the surface, known as the North Equatorial Countercurrent (NECC) and the South Equatorial Countercurrent (SECC). Both of these currents are present in the HOM and in the CSIRO35 simulations, but the NECC is much stronger in the HOM simulation than in the CSIRO35 simulation (Figure 7a,c).

At the equator and beneath the SEC, a strong sub-surface Equatorial Undercurrent (EUC) carries water to the east. The core of the EUC is nearly 200 m deep in the Warm Pool, and it shoals as the EUC flows eastward (Figure 8a). Across the equator, east of the Warm Pool at 180°E, the EUC flows east for depths between 100 m and 300 m, and this is evident in both the HOM and the CSIRO35 simulations (Figure 9a,c). Above the EUC, in the HOM simulation the SEC shoals at the equator, with deeper branches on either side of the equator, whereas in the CSIRO35 simulation the SEC has only one branch with a maximum just south of the equator (Figure 9a,c).

Comparing the simulated zonal currents of the HOM and CSIRO35, one can see that the currents in the HOM simulation are generally stronger and have a more prominent north–south gradient. In particular, the EUC is much stronger in the HOM simulation. To assess the equatorial flow, we compare the simulations with the average zonal current data from the TAO/TRITON mooring at 165°E and 0°S (Figure 10). The figure clearly shows that the magnitude and vertical structure of the HOM simulation are much more consistent with the mooring observations than the CSIRO35 simulation. While the HOM simulation does a good job of representing the current profile and magnitude of the EUC in general, the HOM-simulated EUC is about 20 m shallower than that in the mooring data. This may reflect either a bias in the model or a mismatch in time, as the mooring data comes from the 2000s rather than the 1990s period simulated by the HOM. That the HOM simulation has stronger equatorial currents, with more defined structure, is a clear difference between it and the CSIRO35 present-day simulation, and is an aspect where it is in better agreement with the observations.

4.4. Phytoplankton

To assess the phytoplankton field produced by the simulations, we compare the simulated annual mean phytoplankton concentrations with chlorophyll *a* concentrations estimated from the Sea-viewing Wide Field-of-view Sensor (SeaWiFS) 1997–2008 mean climatology of eight-day, 9 km composites generated by the NASA Goddard Space Flight Center. To perform the comparison, we first convert the simulated phytoplankton concentrations to chlorophyll *a* concentrations (expressed in nitrogen units) by using a conversion factor of 1 mmol N/1.59 mg Chla (Matear, 1995). Within the Warm Pool, the HOM-simulated mean chlorophyll *a* concentrations are low (less than 0.15 mg Chla/m^3) but slightly greater than the observed values, which are less than 0.10 mg Chla/m^3 (Figure 11a,b). To the east of the Warm Pool, both the HOM-simulated and the observed chlorophyll *a* concentrations show their highest values. However, the HOM-simulated values (0.35 mg Chla/m^3) are slightly greater than the observed values (0.30 mg Chla/m^3). The CSIRO-35-simulated concentrations, on the other hand, are more than double the observed values at 140°W (Figure 11a,c). Within the Indonesian Seas, both the simulated and observed fields show mean chlorophyll *a* concentrations that are generally higher than 0.3–0.4 mg Chla/m^3.

In general, both models overestimate the chlorophyll *a* concentrations (Figure 11), but the CSIRO35 simulation has a much greater chlorophyll *a* concentration gradient along the equator, with too-high concentrations in the eastern part of the region. The HOM-simulated spatial distribution of chlorophyll *a* is consistent with the data from SeaWiFS ($r = 0.75$), showing a similar magnitude of variability and small difference from the observations (RMS difference of 0.06 mg Chla/m^3), which gives us some confidence that the HOM provides a realistic representation of the processes controlling phytoplankton variability in the western tropical Pacific. In contrast, the CSIRO35 simulation shows lower correlation with the data, with greater spatial variability and a greater difference from the observations ($r = 0.7$ and RMS difference of 0.15 mg Chla/m^3). We emphasise, however, that the chlorophyll *a* comparison can be problematic for several reasons. First, the conversion of modelled phytoplankton concentration (in nitrogen units, mmol N/m^3) to chlorophyll *a* concentration (mg Chla/m^3) assumes a fixed ratio, but the actual ratio is expected to vary (Taylor et al., 1997). Second, satellite-derived chlorophyll *a* concentrations are based on estimates of water-leaving radiances, which are sensitive to the effects of poorly determined corrections of the atmosphere on these radiances. Third, satellite-derived calculations tend to overestimate chlorophyll *a* concentrations near the coast, because of the influence of dissolved organic matter and sediment resuspension (Moore et al., 2007). Fourth, the nominal uncertainty in the SeaWiFS estimates of chlorophyll *a* concentrations in the open ocean water is ±25–35% (Behrenfeld et al., 2006). Because of these uncertainties in the observations, in our assessment of the HOM simulation we focus on the spatial pattern rather than the magnitude of simulated chlorophyll *a* concentrations.

Along the equator, both the HOM- and CSIRO35-simulated phytoplankton concentrations for the 1990s show high surface values in the eastern part of the section, with a deep phytoplankton maximum existing beneath the Warm Pool (Figure 12a,c). To produce a deep phytoplankton maximum, sufficient light and nutrients are needed to sustain the phytoplankton. The exponential decline in light levels with depth and the presence of the subsurface phytoplankton maximum combine to reduce light levels below the phytoplankton maximum and help confine the deep phytoplankton maximum to a thin layer, thus preventing the occurrence of phytoplankton below a depth of 110 m. While not allowing the simulated phytoplankton to adapt to the low-light conditions beneath the deep phytoplankton maximum helps to limit the extent of this layer in the model, it is a real feature of the Warm Pool region and is observed to be only tens of metres thick (Maes et al., 2010).

The east–west gradient in the simulated phytoplankton concentrations and the existence of a deep chlorophyll maximum in the Warm Pool are both consistent with observations (Le Borgne et al., 2002). The presence in the HOM simulations of a deep phytoplankton maximum to the east of the Warm Pool (east of 170°E) is also observed in chlorophyll data. In this region, the observed deep chlorophyll maximum exceeds 0.3 mg Chla/m^3 (Maes et al., 2010), which is similar to the HOM-simulated values.

While both the HOM and the CSIRO35 simulations produce a deep phytoplankton maximum along the equator, this feature is more extensive in the HOM simulation, which is more consistent with observations. Further, the phytoplankton concentrations in the HOM simulation have smaller magnitude, which is also more consistent with the observations than the CSIRO35 simulation. The CSIRO35 simulation, with its cold tongue bias, has too much upwelling of high-nutrient water in the eastern equatorial Pacific, and this has the effect of maintaining much higher phytoplankton concentrations in the eastern half of the section than what is observed. In the CSIRO35 simulation, upwelling of nutrients and their westward transport supply the nutrients for phytoplankton growth along the equator. The HOM simulation does have upwelling, but the presence of a deep phytoplankton maximum along the equatorial section implies that nutrient supply to the photic zone from below is occurring along the entire section. In the HOM simulation, the existence of a strong vertical zonal current shear along the equator (Figure 8) provides a mixing mechanism for supplying nutrients to the photic zone, which lies below the mixed layer, and hence producing a sub-surface phytoplankton maximum.

5. Climate Change Results and Discussion

In the following discussion, we define the climate change projected by the HOM or by the CSIRO35 as the difference between the simulated ocean states of the 2060s and the 1990s (i.e. 2060s state minus 1990s state). For the HOM, we use monthly averages of the last five years of each 10-year period of simulation; for CSIRO35, we use decadal averages for both periods. We shall compare the HOM and CSIRO35 simulations with each other and with recent analyses of global climate model projections (e.g. Brown et al., 2013a; Ganachaud et al., 2013) as well as observed multi-decadal trends in the region. We will also use the HOM simulation with windstress feedback to assess how interactions between the ocean and atmosphere could modify future climate change projections.

5.1. Changes in Temperature, Salinity and Mixed-Layer Depth

The HOM climate change projection for the western tropical Pacific shows considerable surface warming, with the greatest warming occurring along the equator in the east Pacific and the least warming in the west (Figure 13a). DiNezio et al. (2009) analysed multiple climate model projections and also found the global warming maximum to occur along the equator east of 150°W. Using the dynamic Warm Pool edge definition of Brown et al. (2013b), the Warm Pool regions of the two models for the 1990s and 2060s are shown in Figure 13. In the HOM projection, there is an eastward migration of the Warm Pool with climate change, and the greatest warming occurs along the equator in the expanded Warm Pool region (Figure 13a). The HOM projects less than 2°C surface warming in the Warm Pool, but the warming is in excess of 3°C just east of the 1990s Warm Pool edge. CSIRO35 projects a similar magnitude and pattern of warming, with maximum warming taking place along the equator east of the 1990s Warm Pool edge (Figure 13b). CSIRO35 also projects an eastward movement of the Warm Pool along the equator (Figure 13b).

Along the equator, both the HOM and CSIRO35 project the greatest warming to occur in the upper 100 m, while in the Warm Pool region the projections show prominent sub-surface cooling (up to 1°C) in the thermocline, revealing an uplift of the thermocline (Figure 5). CSIRO35 projects a similar magnitude of warming to the HOM (Figure 5b,d), but the maximum warming and maximum sub-surface cooling occur further west than in the HOM projection, which is consistent with the model having a 1990s Warm

Pool edge which was further west than that of the HOM (160°E compared to 170°E). Ganachaud et al. (2013) showed that the projected multi-model mean (MMM) warming of the CMIP3 climate models was generally restricted to the upper ocean, with warming of 2.5°C at 50 m and 1°C at 100 m between the 1990s and the 2100s. The projected MMM warming lacked the sub-surface cooling at the equator beneath the Warm Pool, but this may reflect the longer time period that Ganachaud et al. (2013) used to compute the warming (1990s to 2100s, compared with 1990s to 2060s in our study).

The surface waters of the HOM and CSIRO35 projections show the greatest freshening in the western tropical Pacific; freshening declines to nearly zero east of the Warm Pool (Figure 14). The freshening of the surface has a very similar pattern in the two simulations and is consistent with observed historical trends, which reveal a multi-decadal decline in salinity in the Warm Pool (Cravatte et al., 2009; Durack et al., 2012). In the Warm Pool at the equator, both models project that the freshening will extend down to 200 m, while east of the Warm Pool the salinity decline is projected to be small. In the HOM projection the freshening in the Warm Pool is deeper, and there is also greater freshening outside the Warm Pool than in the CSIRO35 projection (Figure 6).

Both climate change projections show a general shoaling of the MLD, with the maximum decline being less than 30 m (Figure 15). In the HOM projection, the greatest shoaling occurs near the eastern edge of the Warm Pool (maximum decline of less than 30 m). The CSIRO35 simulation also projected the largest declines in MLD to occur around the edge of the Warm Pool, but these changes appear to be greatest just off the equator (20 m decline), and along the equator the change in MLD is nearly zero.

Observational data from 1950 to 2008 showed that the maximum warming of the western tropical Pacific occurred near the eastern edge of the Warm Pool (Johnson and Wijffels, 2011), so both climate change projections are consistent with this observation. In the Warm Pool, observed water temperatures have decreased by up to 2°C in the thermocline (100–150 m) over 58 years (Johnson and Wijffels, 2011; Durack and Wijffels, 2010); a similar pattern of cooling is produced by the HOM and CSIRO35 climate change projections, but the projected magnitude of cooling is less, at only 1°C. Such cooling seems to be related to a weakening of the easterly equatorial winds, which causes an adiabatic lifting of the thermocline (Han et al., 2006). Weakening of the easterly equatorial winds is a robust feature of future climate change projections (Collins et al., 2010), and it is present in the climate change projection used to force the HOM. The HOM-projected uplift of the thermocline in the Warm Pool is consistent with the observed trend over the past 50 years and with the expected response due to climate change.

5.2. Change in Equatorial Currents

With climate change, along the equator both the HOM and CSIRO35 projected a weakening of the SEC, with the emergence of a weak eastward flow in the Warm Pool (Figure 7b,d). However, in the CSIRO35 projection these changes in the zonal flow are smaller and more diffuse than in the HOM projection. Below the surface, the EUC is still prominent in the 2060s in both the HOM and the CSIRO35 projections (Figure 8b,d). The HOM predicts a less than 5% weakening in its EUC strength, but the core of the EUC is projected to shoal by about 30 m east of the Warm Pool. CSIRO35 predicts similar changes in the EUC strength and position.

In the tropical Pacific, the upper ocean currents are expected to change in the future as a result of weakened equatorial and northeasterly trade winds together with strengthened southeasterly trade winds (Sen Gupta et al., 2012). Ganachaud et al. (2013) showed that according to the MMM, climate change will decrease the velocity of the westward-flowing SEC, from 30 cm/s in the 2000s to 20 cm/s in 2100, which is about double the decline predicted by the HOM climate projections. Ganachaud et al. (2013) also showed that from the MMM, by 2100 the EUC is expected to increase substantially, with an approximately 20 m shoaling of the EUC core. With climate change, the HOM predicted EUC shoaling but little change in its strength. Overall, the HOM projects less change in the EUC and SEC than does the MMM, but this discrepancy may reflect the difference in time periods covered by the studies (the HOM used the 2060s to compute the change, while the MMM used 2100).

5.3. Changes in Phytoplankton

In the western tropical Pacific, the HOM projects a decline in surface phytoplankton concentrations with climate change, except in the Indonesian Seas, where there is a small increase (Figure 16a). The decline in phytoplankton concentration is greatest along the equator near the Warm Pool edge. CSIRO35 also projects a decline in surface equatorial phytoplankton (Figure 16b), but the decline it predicts is much greater than that of the HOM projection. At 100 m depth, the two climate change projections start to differ (Figure 17). CSIRO35 projects a general decline in phytoplankton concentrations, while the HOM projects a band of increased phytoplankton concentrations along the equator across the whole region. Within the Warm Pool, the increase in phytoplankton reflects the shoaling of the thermocline, which raises the nutricline into the photic zone and thus increases phytoplankton concentrations. This feature is most evident in the HOM projection at 150°E; it is weakly present in the CSIRO35 projection but is shifted to the west, at 140°E (Figure 12b,d). Le Borgne et al. (2011) hypothesised that the shoaling of the thermocline with climate change, similar to what occurs during an El Niño (Le Borgne et al., 2011), could increase nutrient supply to the photic zone in the Warm Pool; however, the one climate projection they looked at did not actually produce such a response. Along the equator outside of the Warm Pool, CSIRO35 projected a decline in phytoplankton concentration across the region while HOM projected an increase at 95 m depth across the whole region (Figure 12b,d). The HOM projection suggests that nutrient supply in the western tropical Pacific can increase with climate change.

The HOM-projected increase in phytoplankton concentrations at 100 m approximately cancels the decrease at the surface, and results in primary productivity in the equatorial Pacific remaining nearly unchanged in the HOM projection (Figure 18b). In contrast, primary productivity declines substantially in the CSIRO35 projection (Figure 18d). Like the CSIRO35 projection, other climate models generally project declines in the western tropical Pacific primary productivity with climate change (Steinacher et al., 2010). The discrepancy in the responses of primary productivity to climate change is a significant difference between the two projections. To help understand this difference, let us look at the simulated behaviour along the equator.

Vertical shear mixing along the equator can supply nutrients to the photic zone (Ryan et al., 2002), and in the HOM simulation this occurs in both the 1990s and the 2060s, as demonstrated by the presence of a sub-surface phytoplankton maximum along the equator (Figure 12). Since both the zonal current strengths and the vertical current shears are much stronger in the HOM than in the CSIRO35 simulation (Figure 10), this mechanism is only apparent in the HOM simulation. Without the enhanced vertical and horizontal resolution at the equator, CSIRO35 has much weaker zonal currents with much less vertical current shear, and in this model the eastern equatorial Pacific upwelling of nutrients and their subsequent transport west is the main process supplying nutrients to the equatorial phytoplankton. This is the dominant mechanism of nutrient supply in climate models (Steinacher et al., 2010). As the ocean warms and stratifies and the upwelling declines, CSIRO35 projects a significant decline in phytoplankton concentrations and primary productivity in the western tropical Pacific, consistent with other climate model projections (Steinacher et al., 2010).

In both the HOM and the CSIRO35 projections, the EUC shoals with little change in its strength (Figure 8). In the HOM projection, the shoaling of the EUC increases the vertical current shear and increases vertical shear mixing. The increase in vertical shear mixing increases the nutrient supply to the photic zone and thus increases sub-surface phytoplankton concentrations (Figure 12). Hence, this nutrient supply mechanism can counter the reduction in nutrient upwelling in the eastern equatorial Pacific to yield a small increase in primary productivity. The high resolution in our model is necessary to enable representation of the vertical shear mixing and the subsequent primary productivity response to climate change. The increase in sub-surface phytoplankton in the HOM climate change projection, accompanied by little change in primary productivity, represents an important modification to existing climate change projections and potentially has significant consequences for the marine ecosystem.

5.4. Impact of Projected Climate Change on Tuna Distribution

The warming and changes in primary productivity projected by the model simulations could influence tuna distributions both directly, through changes in preferred thermal environment, and indirectly, through changes in prey abundance. To explore the impact of climate change on tuna distribution, we consider how the projected changes might affect skipjack tuna habitat. By optimising the Spatial Ecosystem And Population Dynamics Model (SEAPODYM), Lehodey et al. (2013) estimated that the preferred thermal range was 26.5–32.5°C for spawning skipjack tuna and 16–25°C for adult skipjack. Defining skipjack habitat as the water column thickness of the tuna's preferred thermal range, we compare the 1990s skipjack habitat from the HOM simulation with observations and with the projections for the 2060s (Figures 19 and 20).

The simulated thickness of the spawning skipjack habitat in the 1990s compares well with the thickness calculated from the CARS2009 mean temperature data (Figure 19a,b). The thickest layer of habitat is found just south of the equator, where it exceeds 140 m. With climate change, the HOM projects that the maximum thickness of the spawning habitat will migrate southward to become centred around 10°S. By bias-adjusting the CSIRO35 climate change projection, we get a preferred spawning habitat which is very similar to that in the HOM projection (Figure 19c,d). The increased resolution of the HOM did not significantly change the projected thickness of the spawning habitat. For comparison, the simulations of Lehodey et al. (2013), using SEAPODYM and a bias-corrected climate change projection, showed that by 2100 the favourable skipjack spawning ground would shift to higher latitudes but also into the central and eastern Pacific. Neither of the climate projections studied here display a large eastward shift, but perhaps this is a feature that emerges only after the 2060s.

The HOM-simulated thickness of the adult skipjack thermal habitat in the 1990s also shows good agreement with observations (Figure 20a,b). The HOM simulation captures the slightly thicker habitat along the equator that is apparent in the observations. With climate change, HOM projects little change in the thickness of the adult thermal habitat ($\pm$10 m) (Figure 20c). CSIRO35 projected a similar thickness of adult habitat to the HOM but with a slightly increased thickness (20 m) in the western equatorial Pacific (Figure 20c,d). What the CSIRO35 projection misses is the narrow band of increased thickness along the equator evident in the HOM projection. The equatorial band of increased adult habitat is associated with the increased vertical shear mixing that occurs in the HOM projection, which led to the increased primary productivity. Lehodey et al. (2013), using the IPSLc climate model projection, predicted that the biomass of adult tuna will shift its core habitat from the western to the central equatorial region by 2100. Our climate projections do not suggest such a shift, but it is possible that this shift may develop only after the 2060s. For the 2060s, our model predicts that across the entire western tropical Pacific, suitable adult skipjack habitat will remain greater than 50 m, which is comparable to the thickness of the 1990s habitat in the Western Pacific Warm Pool (Figure 20a,c).

From the MMM, Ganachaud et al. (2013) concluded that with climate change, skipjack are likely to move substantially eastward and poleward by 2100. While an eastward and poleward extension of the population may occur, we emphasise that in the western tropical Pacific, a region for which little change in the future habitat is projected, one would still expect to find skipjack tuna in the 2060s. Further, given the increase in sub-surface phytoplankton concentrations in a narrow band along the equator, little change in primary productivity, and the continued presence of suitable habitat for adult and spawning skipjack, conditions are such that one would expect to see little change in the 2060s skipjack population. Perhaps, as projected by

Lehodey et al. (2013), future declines in skipjack habitat and biomass will occur only after the 2060s.

The HOM simulation that incorporated windstress feedback predicted a slightly more positive situation for skipjack; that is, in the western equatorial Pacific the adult and spawning thermal habitats were projected to be slightly greater (about 10 m thicker) and the primary productivity about 10% higher along the equator than in the original HOM projection. This modified HOM projection has slightly greater vertical shear mixing caused by the EUC, which increased by about 10% with climate change. While the HOM projected slightly positive conditions for skipjack, other species of tuna with a preference for the Warm Pool could also benefit from the projected changes for the 2060s.

5.5. Robustness of the Climate Projection

To compute the climate projection with the HOM, we defined climate change as the difference in the CSIRO35-simulated climate state between the 1990s and the 2060s. Given the potential for multi-decadal variability in the western tropical Pacific, it is possible that our simulations are biased because we derived climate change from the difference between the climate states of two decades. To assess decadal bias, we compare the change in zonal windstress between the 1990s and the 2060s with the difference derived from a three-decade average centred on the periods of interest; that is, we use the difference between the years 1980–2009 and the years 2050–2079 to compute climate change (Figure 21a,b). The magnitude and pattern of change are very similar for the two calculations. A similar comparison was also made for the windstress curl (Figure 21c,d), and we again found good agreement in the pattern and magnitude for the two calculations. The similarity of the windstress changes demonstrates that our climate change estimate is unlikely to have been biased by multi-decadal variability.

In the HOM projection, a key driver of the increase in the deep phytoplankton maximum along the equator and the weak response of primary productivity to climate change was the shoaling of the EUC. This change increased the vertical current shear and increased vertical shear mixing. Analysis of multiple climate projections suggests both shoaling of and an increase in the EUC with climate change (Sen Gupta et al., 2012). Sen Gupta et al. (2012) showed that the strengthening of the EUC is purely a wind-driven response to the projected intensification of southeasterly trade winds and an associated off-equatorial windstress curl change in the southern hemisphere.

CSIRO35 projects a small reduction in the EUC strength, as opposed to most other models, which have shown that the EUC increases with climate change (Sen Gupta et al., 2012); in particular, the MMM exhibits a substantial strengthening of the EUC with climate change (Ganachaud et al., 2013). A greater increase in EUC strength should further increase vertical shear mixing and hence the supply of nutrients to the photic zone along the equator. Therefore, because CSIRO35 did not project a substantial increase in EUC strength, the HOM projection here may be underestimating the vertical shear mixing and the potential for climate change to increase phytoplankton concentrations and primary productivity in the western tropical Pacific. The HOM climate change projection with windstress feedback has an EUC that increased by about 10%, and it did lead to slightly greater primary productivity.

6. Summary

For most of the physical environmental variables, the 2060s HOM climate projection was similar to the CSIRO35 projection. Enhanced resolution and bias correction appear to have only a minor impact on the climate change projection of the physical ocean state. Both low- and high-resolution climate projections showed a maximum surface warming east of the Warm Pool, a shoaling of the thermocline in the Warm Pool, and eastward expansion of the Warm Pool. In the Warm Pool, the shoaling of the thermocline raises the nutricline into the photic zone and increases phytoplankton and primary productivity, a feature that is most evident in the HOM projection but is also weakly present in the CSIRO35 projection.

Where the HOM projection displayed a clear difference from the CSIRO35 projection was in the impact of climate change on phytoplankton concentrations. For phytoplankton, the enhanced resolution of the HOM had an important effect. The HOM simulation had stronger and better-defined zonal currents than the CSIRO35 simulation, and this enabled vertical current shear mixing to play an important role in generating a phytoplankton sub-surface maximum along the equator in the Western Pacific. The HOM projected a shoaling of the EUC with climate change, which enhanced the vertical shear mixing and increased the vertical supply of nutrients to the photic zone, resulting in an increase of sub-surface phytoplankton concentrations. The increase in sub-surface phytoplankton concentrations helped to offset the decline in surface phytoplankton and to produce simulation results showing almost no change in primary productivity in the western tropical Pacific with climate change. In contrast, CSIRO35 projected a substantial reduction in phytoplankton concentrations and primary productivity, a response that is typical of climate change projections for the region (Steinacher et al., 2010).

The projected expansion of the Warm Pool along with little projected change in primary productivity and in suitable habitat for skipjack tuna suggest that by the 2060s, climate change will not have had an adverse impact on skipjack tuna populations. Beyond the 2060s the situation may be different, as suggested by Lehodey et al. (2013), but there is a need to repeat their study using a high-resolution model that can resolve current shear mixing and its response to climate change.

An important limitation of the HOM is that the simulations were not dynamically coupled to the atmosphere. Chamberlain et al. (2012) used simulations with varying heat, freshwater and windstress coupling of the HOM with the atmosphere to assess the robustness of the HOM climate change projection. These sensitivity experiments showed that the pattern of phytoplankton change was robust (with a spatial correlation of 0.8 between projections), and there was a slight amplification of the response (10% increase) when the feedback of the ocean state on the windstresses was included in the simulations. While Chamberlain et al. (2012) in their sensitivity experiments probed the impact of changes in ocean warming on atmospheric dynamics, they did not investigate the response of the coupled system. Given the importance of atmosphere–ocean coupling in the western tropical Pacific, there is a need to undertake global climate model simulations with a high-resolution ocean model. Such simulations should also investigate how ENSO variability is affected by climate change.

Acknowledgements

We would like to thank the Ocean Biology Processing Group at the NASA Goddard Space Flight Center, Greenbelt, Maryland, USA, for their production and distribution of the SeaWiFS ocean colour dataset. We acknowledge the free access to the TAO/TRITON data, a joint effort between PMEL and JAMSTEC; the data are available at www.pmel.noaa.gov/tao and www.jamstec.go.jp. Funding for this work was provided by the Pacific Climate Change and Adaptation Program, the Australian Climate Change Science Program, the CSIRO Wealth from Ocean Flagship, the CSIRO Climate Adaptation Flagship and the Western Australia Marine Science Initiative. Part of this research was undertaken at the NCI National Facility in Canberra, Australia, which is supported by the Australian Commonwealth Government.

7. Figures

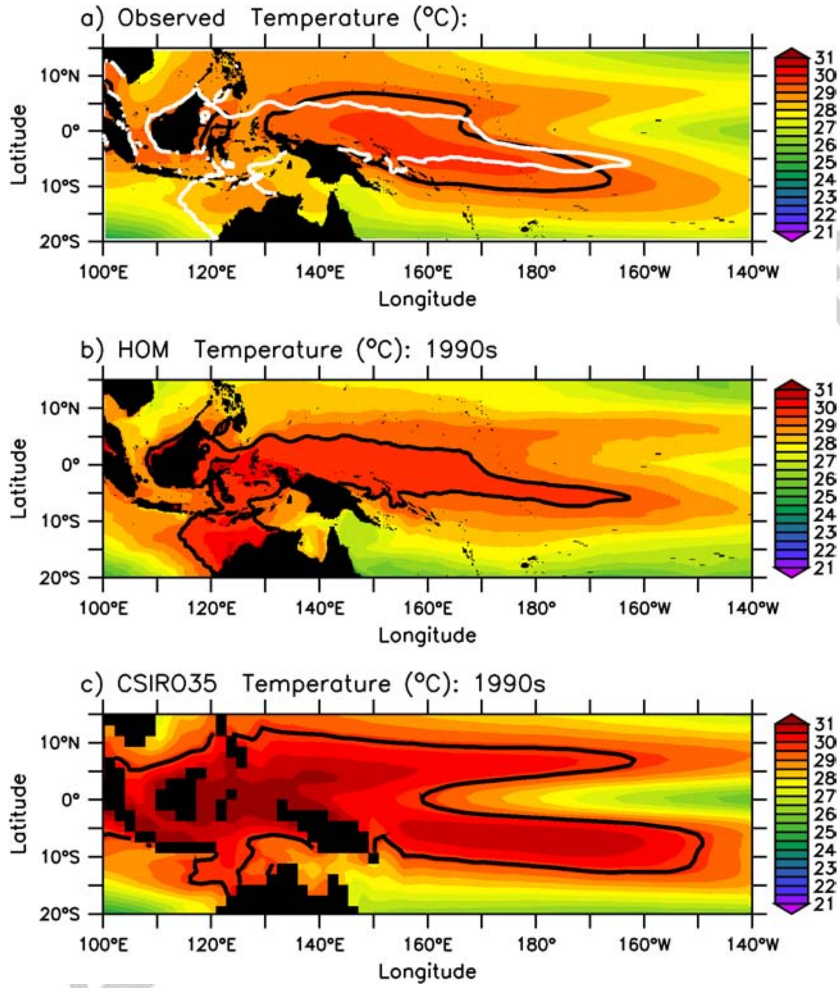

Figure 1: Annual mean sea surface temperature (°C) from a) the observations of Reynolds and Smith (1994), b) the HOM simulation for the 1990s, and c) the CSIRO35 simulation for the 1990s. The thick black lines represent the dynamic Warm Pool edge (Brown et al., 2013b) for the three datasets. The thick white line in a) shows the dynamic Warm Pool edge in the 1990s HOM simulation.

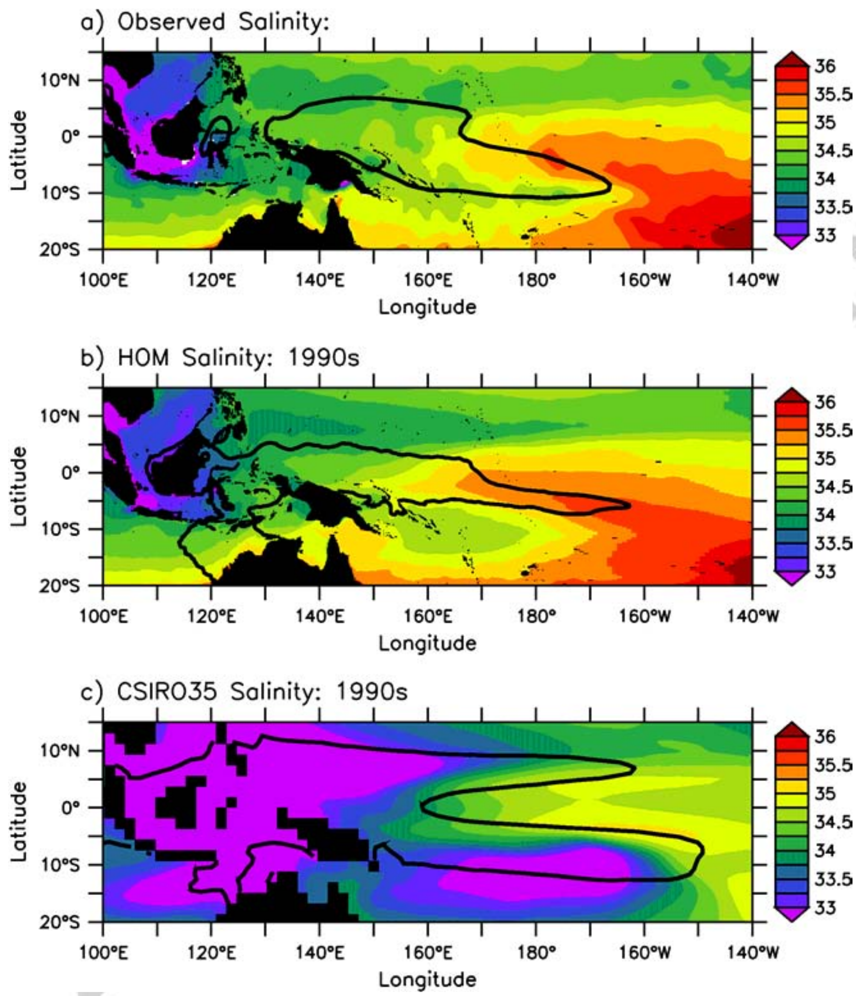

Figure 2: Annual mean sea surface salinity from a) the observations based on CARS2009, b) the HOM simulation for the 1990s, and c) the CSIRO35 simulation for the 1990s. The thick black lines represent the dynamic Warm Pool edge (Brown et al., 2013b) for the three datasets.

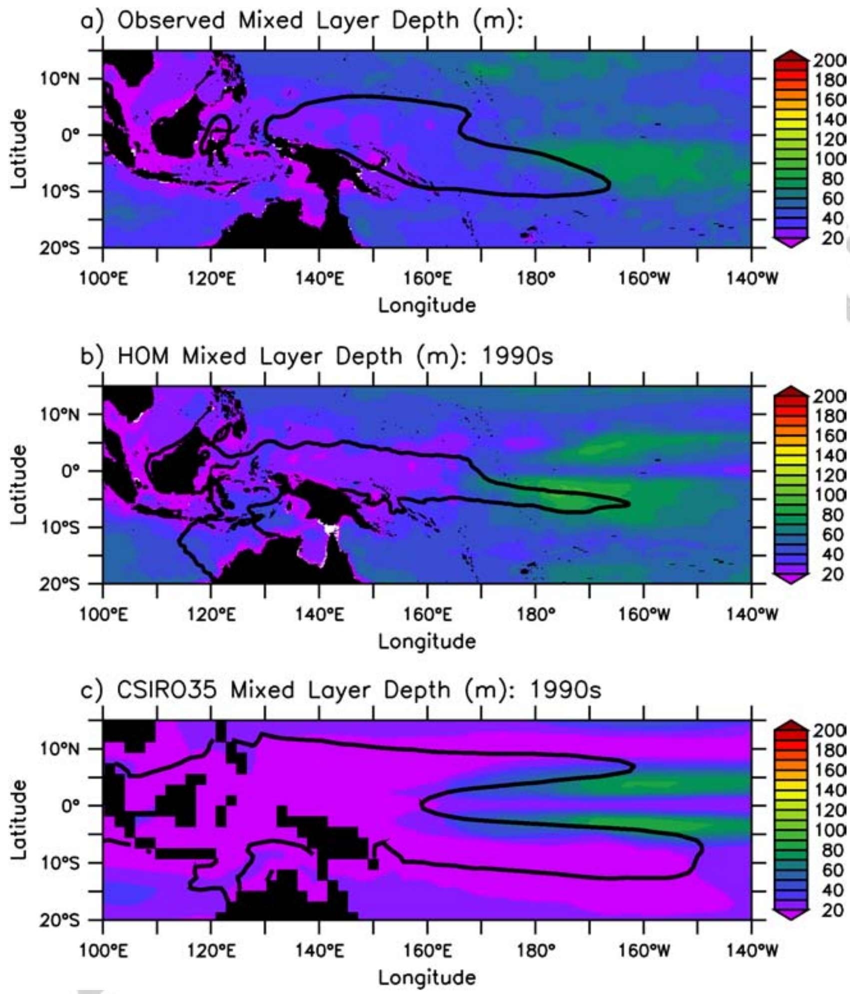

Figure 3: Monthly averaged mixed-layer depth (m) from a) the observations based on CARS2009, b) the HOM simulation for the 1990s, and c) the CSIRO35 simulation for the 1990s. The thick black lines represent the dynamic Warm Pool edge (Brown et al., 2013b) for the three datasets.

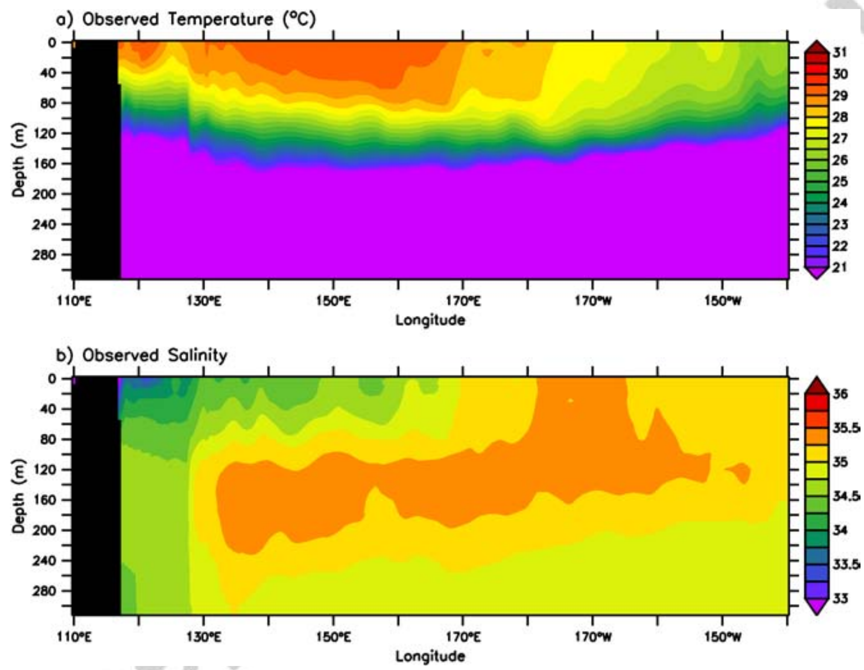

Figure 4: Observations along the equator (between 3°N and 3°S) from the CARS2009 climatology: a) annual mean temperature (°C); b) annual mean salinity.

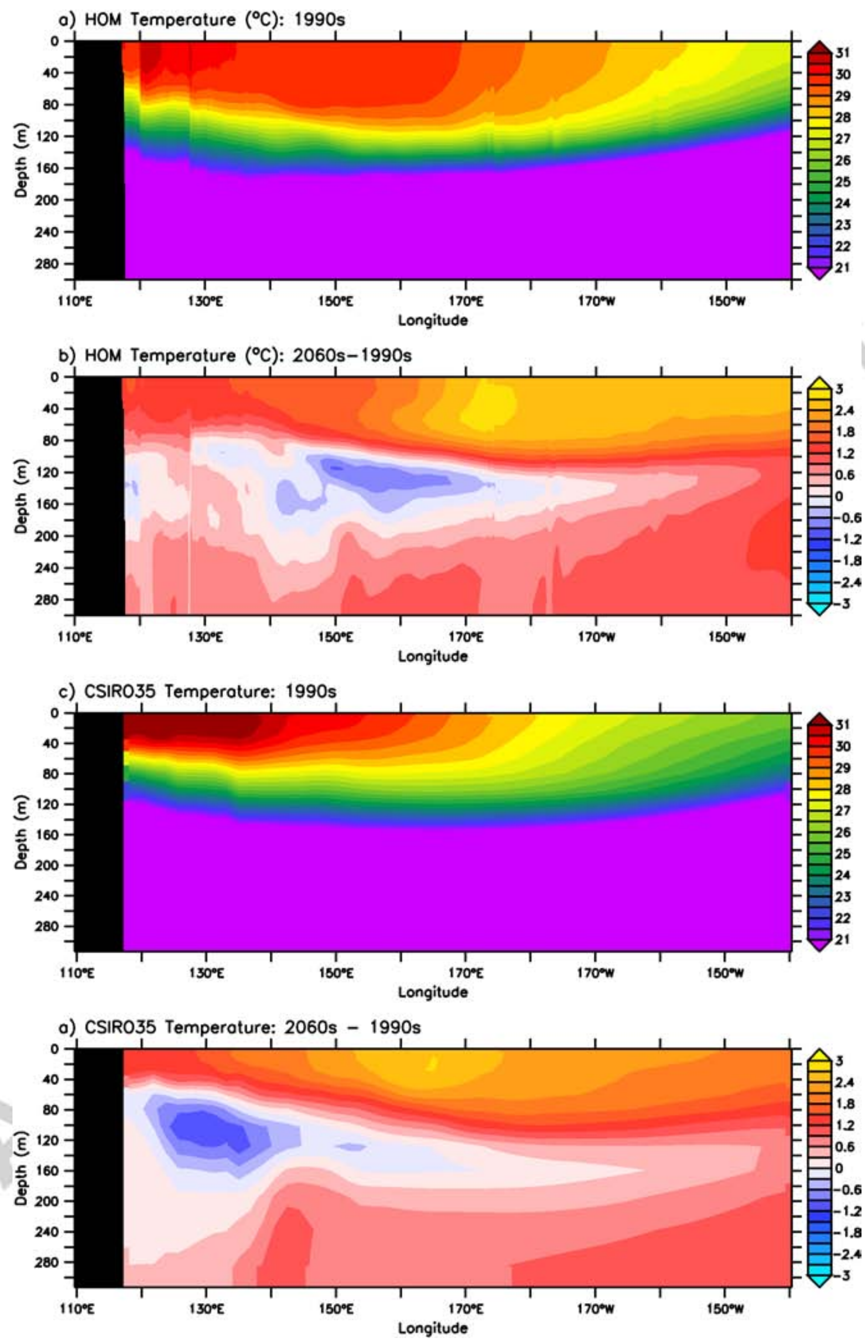

Figure 5: Simulated averaged mean temperature (°C) along the equator (between 3°N and 3°S): a) temperatures from the 1990s HOM simulation; b) difference between temperatures of the 2060s and the 1990s obtained from the HOM projection; c) temperatures from the 1990s CSIRO35 simulation; d) difference between temperatures of the 2060s and the 1990s obtained from the CSIRO35 projection.

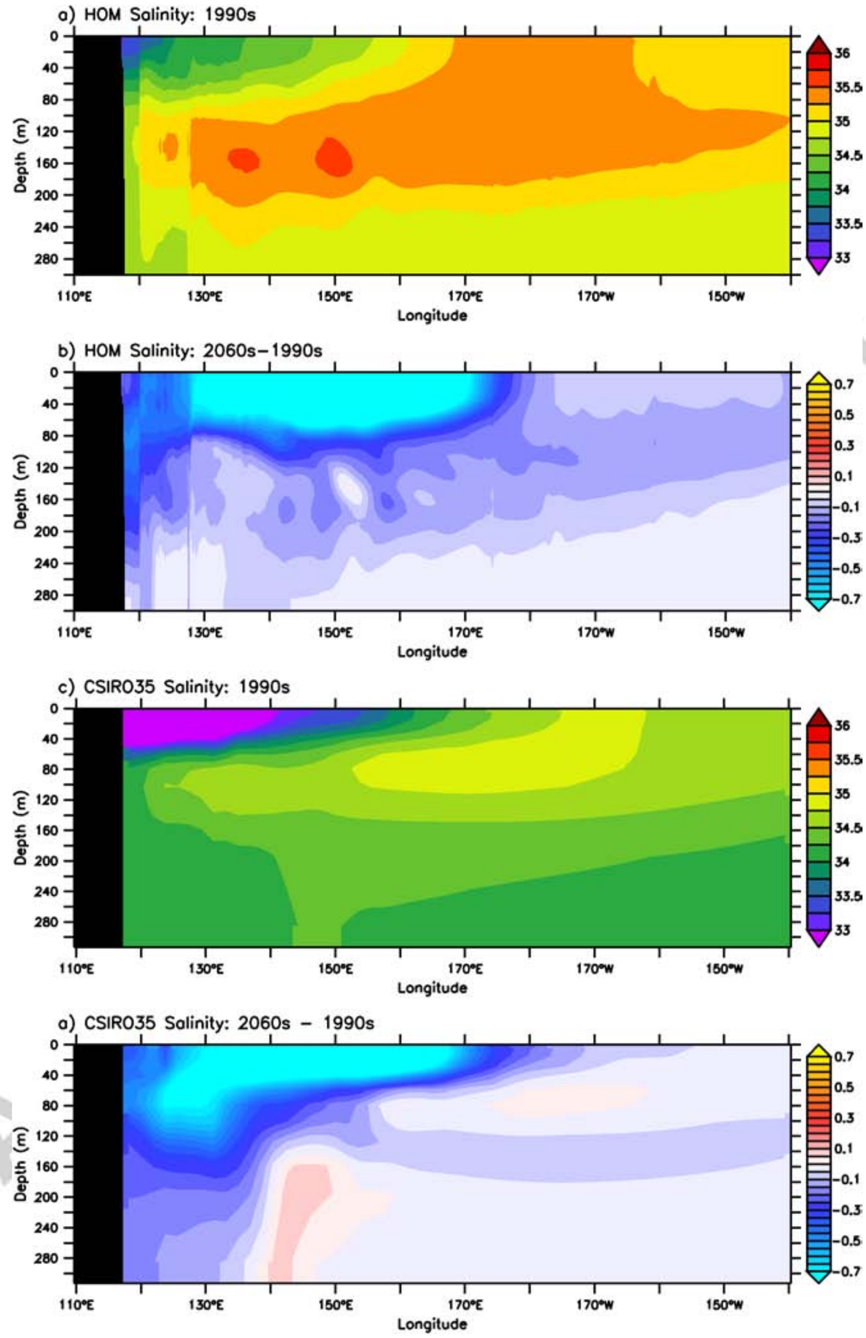

Figure 6: Simulated annual averaged salinity along the equator (between 3°N and 3°S): a) salinities from the 1990s HOM simulation; b) difference between salinities of the 2060s and the 1990s obtained from the HOM projection; c) salinities from the 1990s CSIRO35 simulation; d) difference between salinities of the 2060s and the 1990s obtained from the CSIRO35 projection.

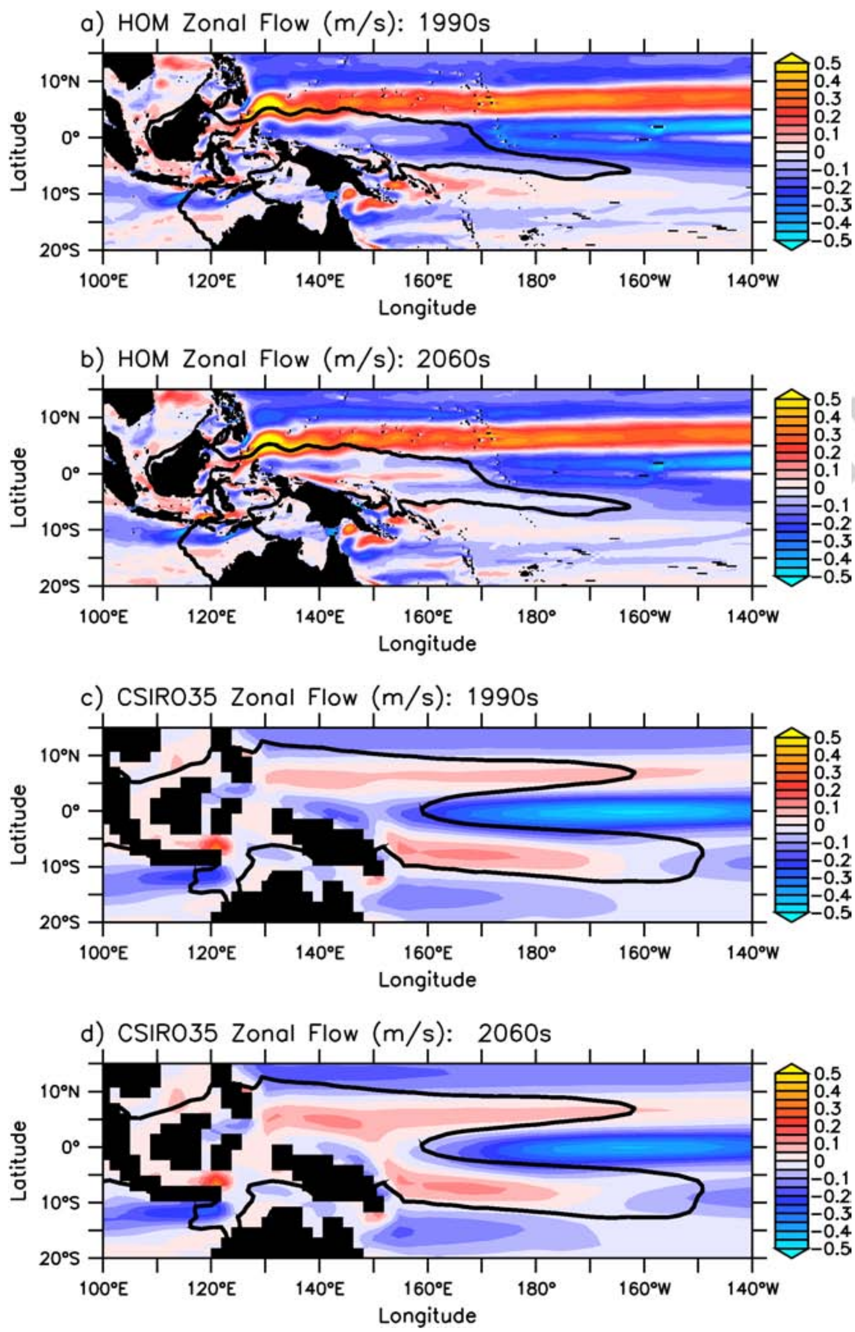

Figure 7: Annual averaged upper ocean (0–50 m) mean zonal flow obtained from a) HOM simulation for the 1990s, b) HOM simulation for the 2060s, c) CSIRO35 simulation for the 1990s, and d) CSIRO35 simulation for the 2060s. The thick black lines represent the dynamic Warm Pool edge (Brown et al., 2013b) of the 1990s in the respective simulations.

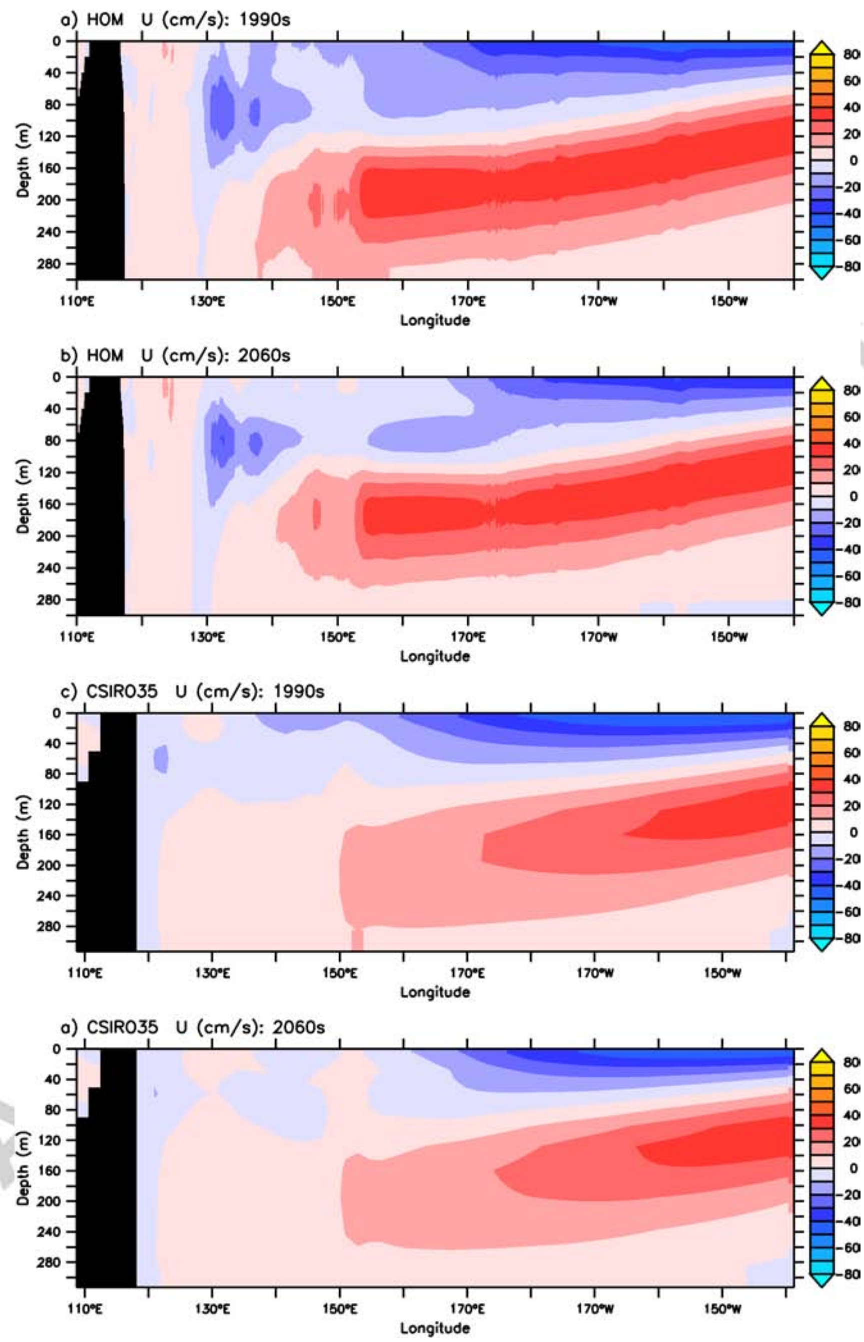

Figure 8: Simulated eastward velocity (cm/s) along the equator (between 3°N and 3°S), obtained from a) HOM simulation for the 1990s, b) HOM simulation for the 2060s, c) CSIRO35 simulation for the 1990s, and d) CSIRO35 simulation for the 2060s.

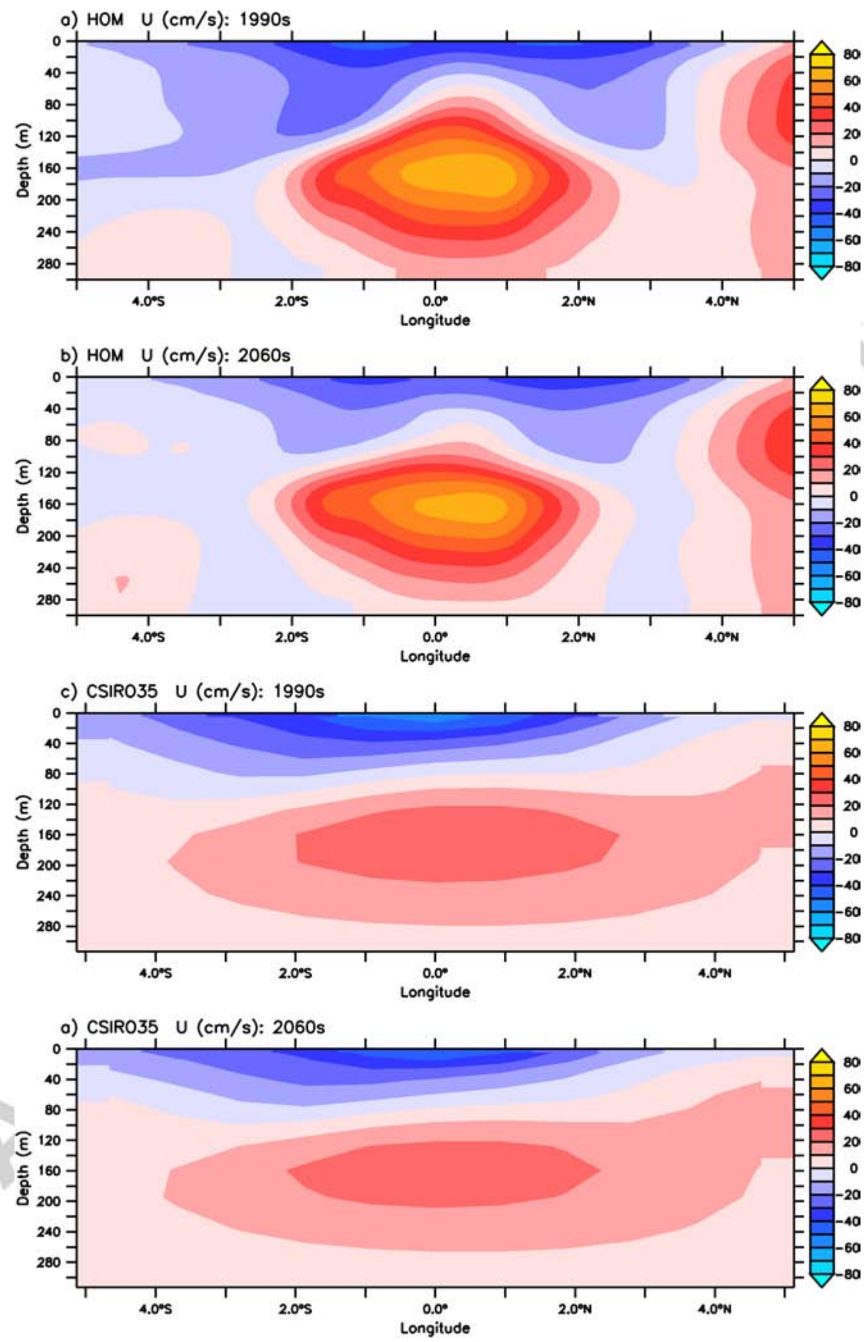

Figure 9: Simulated eastward velocity (cm/s) at 180°E, obtained from a) HOM simulation for the 1990s, b) HOM simulation for the 2060s, c) CSIRO35 simulation for the 1990s, and d) CSIRO35 simulation for the 2060s.

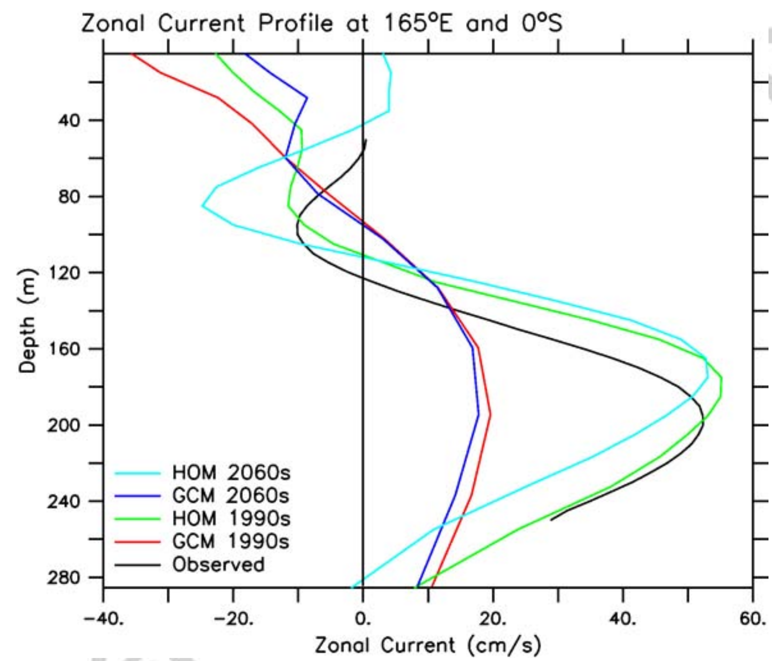

Figure 10: Observed zonal averaged current profile (cm/s) at the TAO/TRITON current mooring site (165°E and 0°S), along with simulated values from the HOM and CSIRO35 for the 1990s and 2060s.

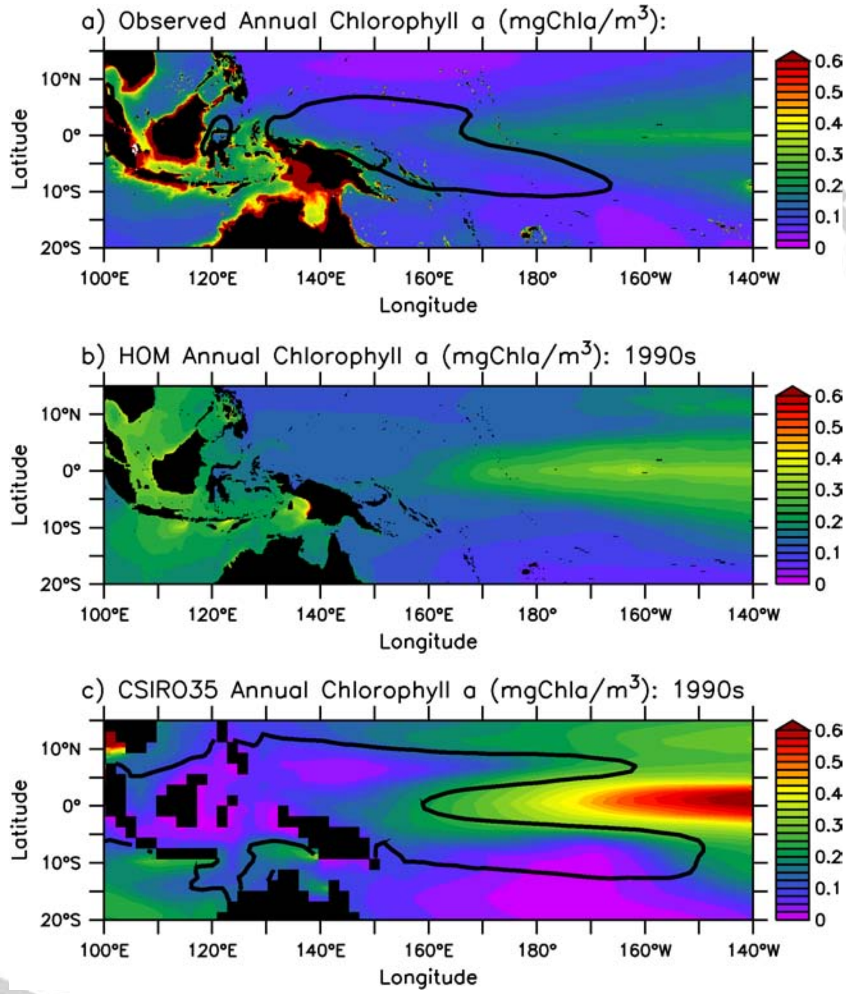

Figure 11: Annual mean surface chlorophyll a concentration (mg Chla/m^3): a) computed from 1997–2008 eight-day, 9 km composites of SeaWiFS; b) obtained from the 1990s HOM simulation; c) obtained from the 1990s CSIRO35 simulation. The thick black lines represent the dynamic Warm Pool edge (Brown et al., 2013b) of the 1990s from the observations and the respective simulations.

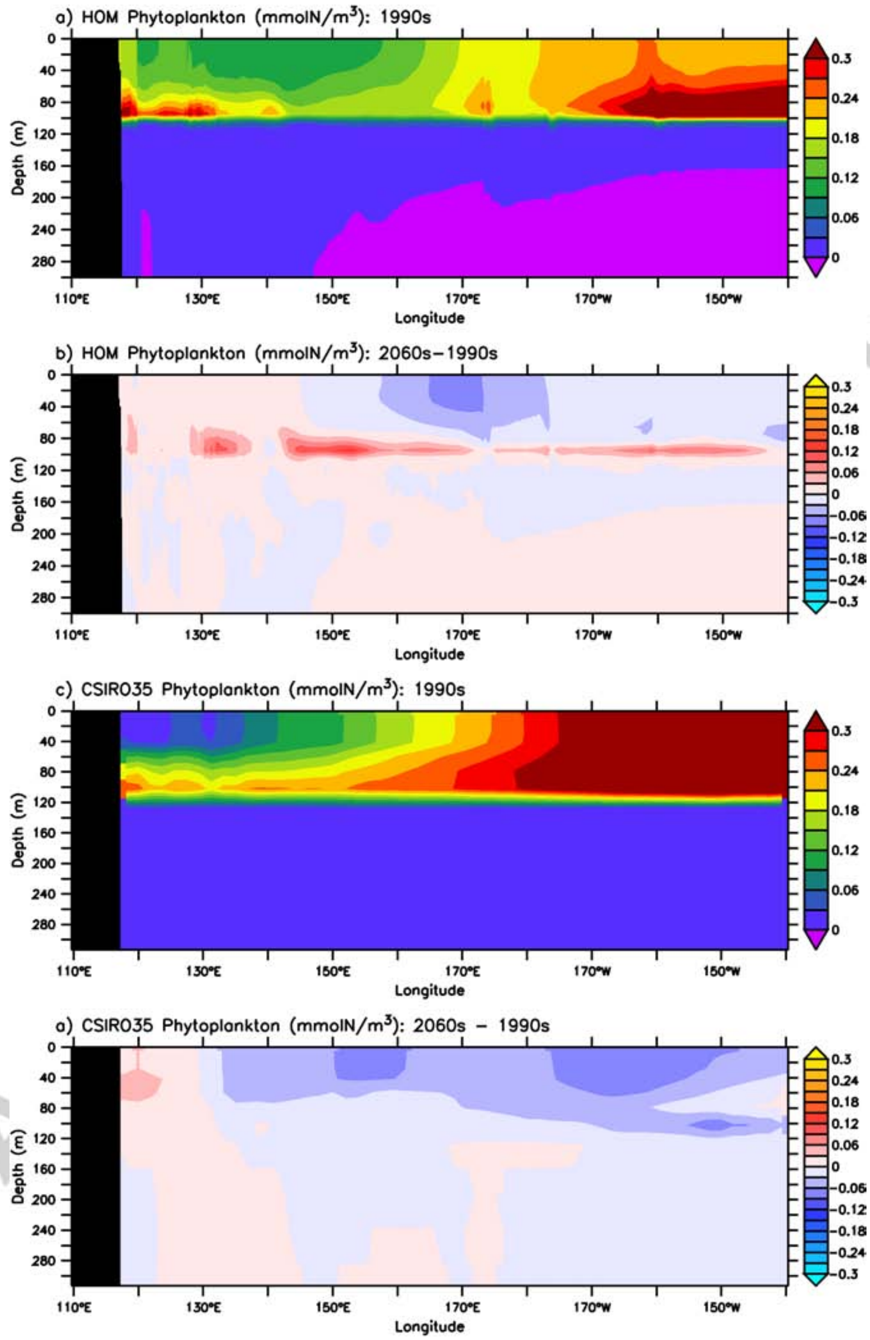

Figure 12: Simulated annual average phytoplankton concentration (mmol N/m^3) along the equator (between 3°N and 3°S): a) concentrations from the 1990s HOM simulation; b) difference between concentrations of the 2060s and the 1990s obtained from the HOM projection; c) concentrations from the 1990s CSIRO35 simulation; d) difference between concentrations of the 2060s and the 1990s obtained from the CSIRO35 projection.

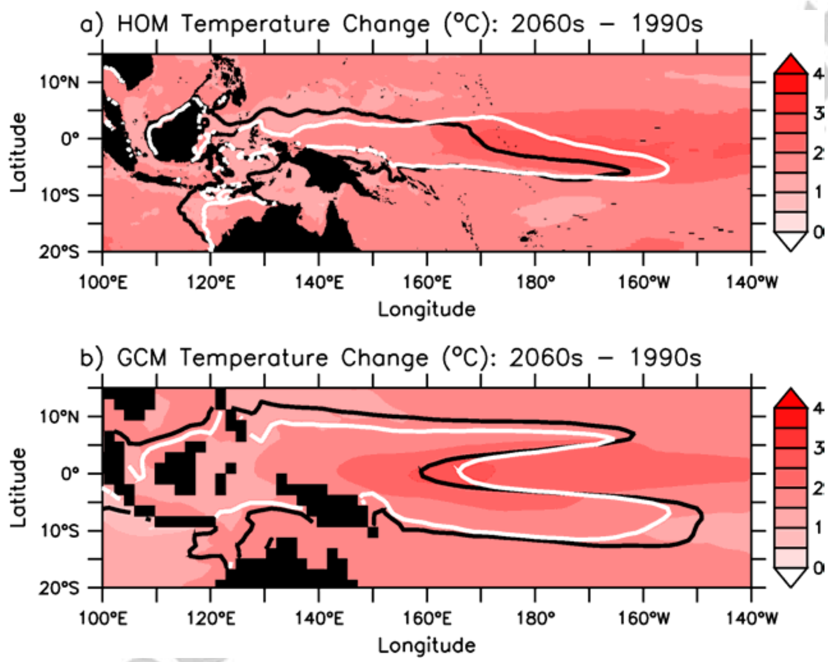

Figure 13: Projected annual averaged change in sea surface temperature between the 1990s and the 2060s, obtained from a) the HOM simulation and b) the CSIRO35 simulation. The thick black (white) lines represent the dynamic Warm Pool edge (Brown et al., 2013b) of the 1990s (2060s) in the respective simulations.

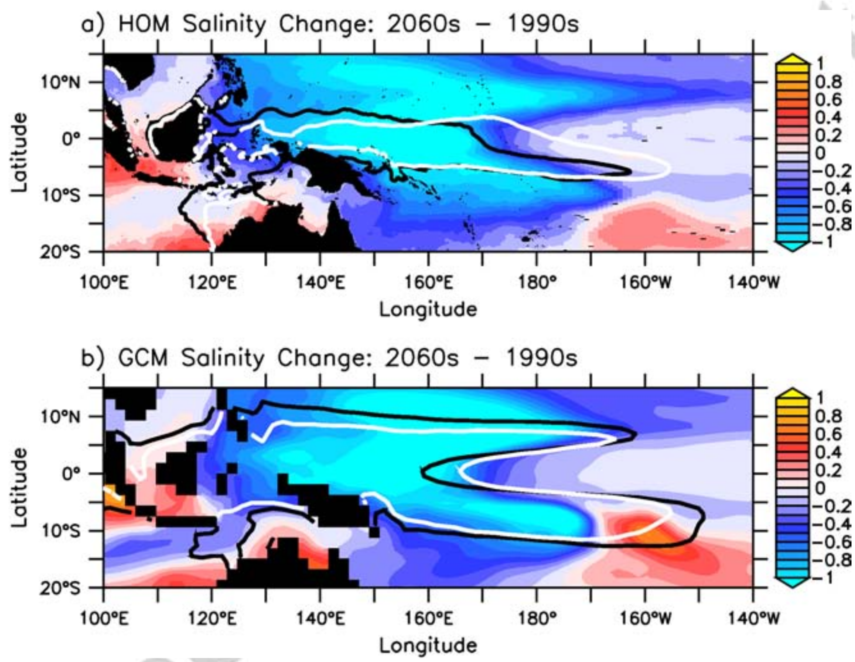

Figure 14: Projected annual averaged change in sea surface salinity between the 1990s and the 2060s, obtained from a) the HOM simulation and b) the CSIRO35 simulation. The thick black (white) lines represent the dynamic Warm Pool edge (Brown et al., 2013b) of the 1990s (2060s) in the respective simulations.

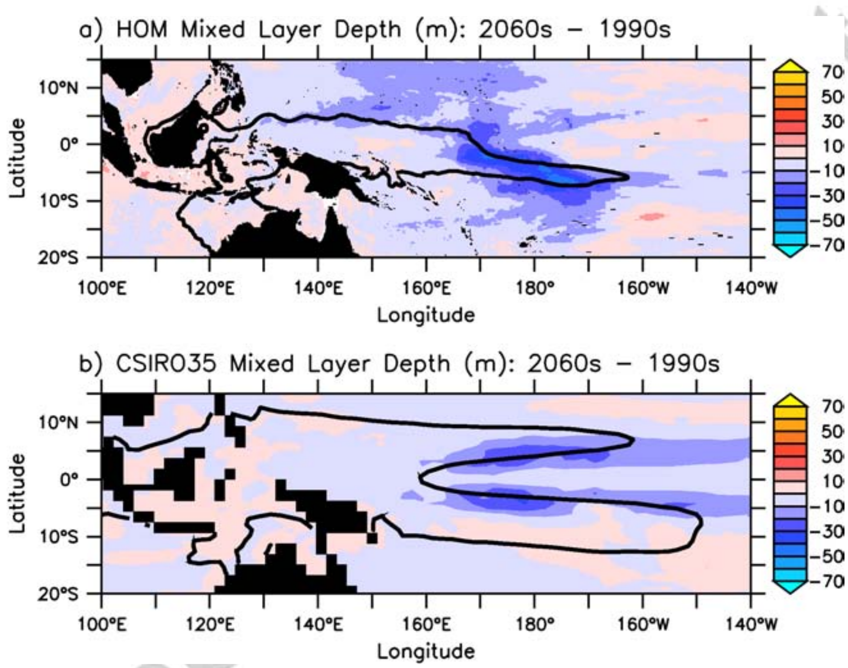

Figure 15: Projected change in the annual mean mixed-layer depth (m) between the 1990s and the 2060s, obtained from a) the HOM simulation and b) the CSIRO35 simulation. The thick black lines represent the dynamic Warm Pool edge (Brown et al., 2013b) of the 1990s in the respective simulations.

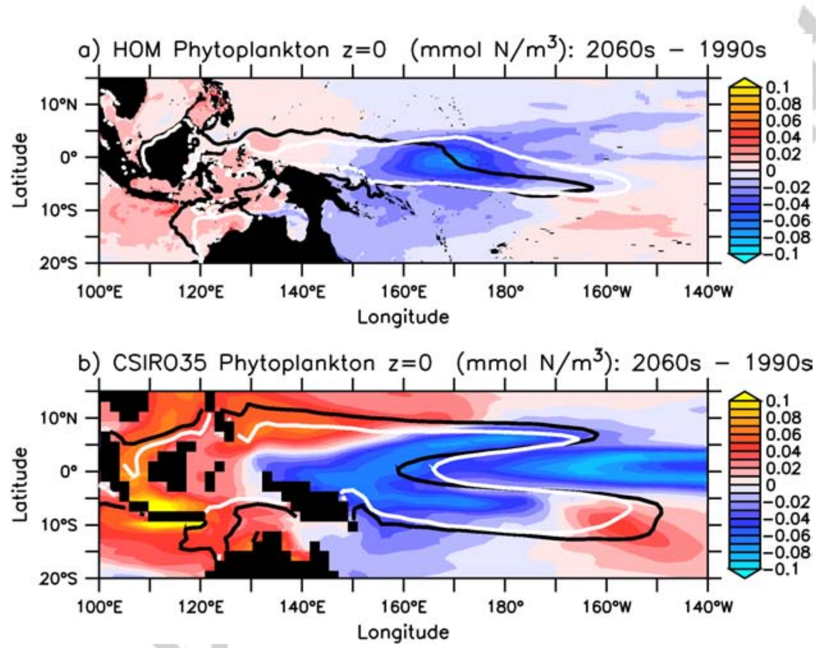

Figure 16: Projected change in annual mean surface phytoplankton concentration (mmol N/m^3) between the 1990s and the 2060s, obtained from a) the HOM simulation and b) the CSIRO35 simulation. The thick black (white) lines represent the dynamic Warm Pool edge (Brown et al., 2013b) of the 1990s (2060s) in the respective simulations.

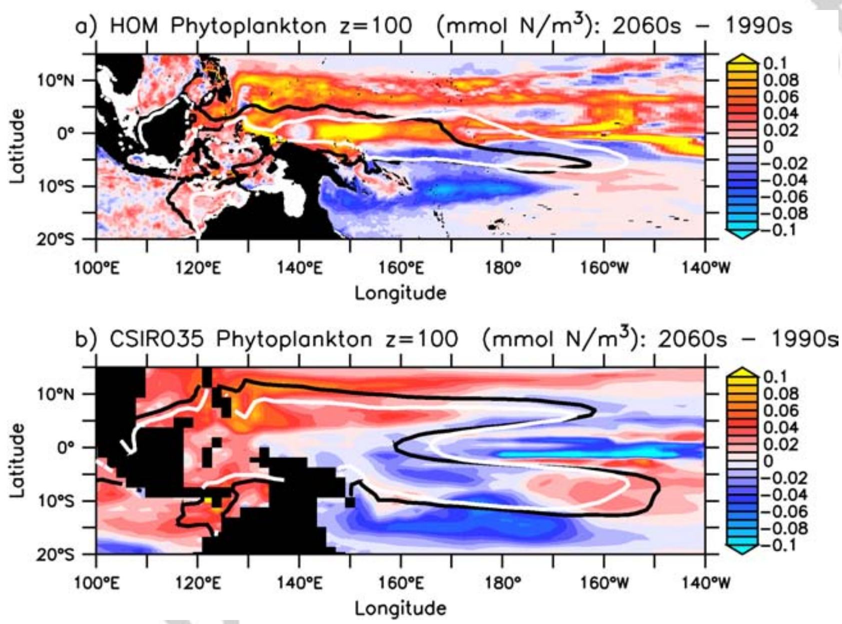

Figure 17: Projected change in annual mean phytoplankton concentration (mmol N/m^3) at a depth of 100 m between the 1990s and the 2060s, obtained from a) the HOM simulation and b) the CSIRO35 simulation. The thick black (white) lines represent the dynamic Warm Pool edge (Brown et al., 2013b) of the 1990s (2060s) in the respective simulations.

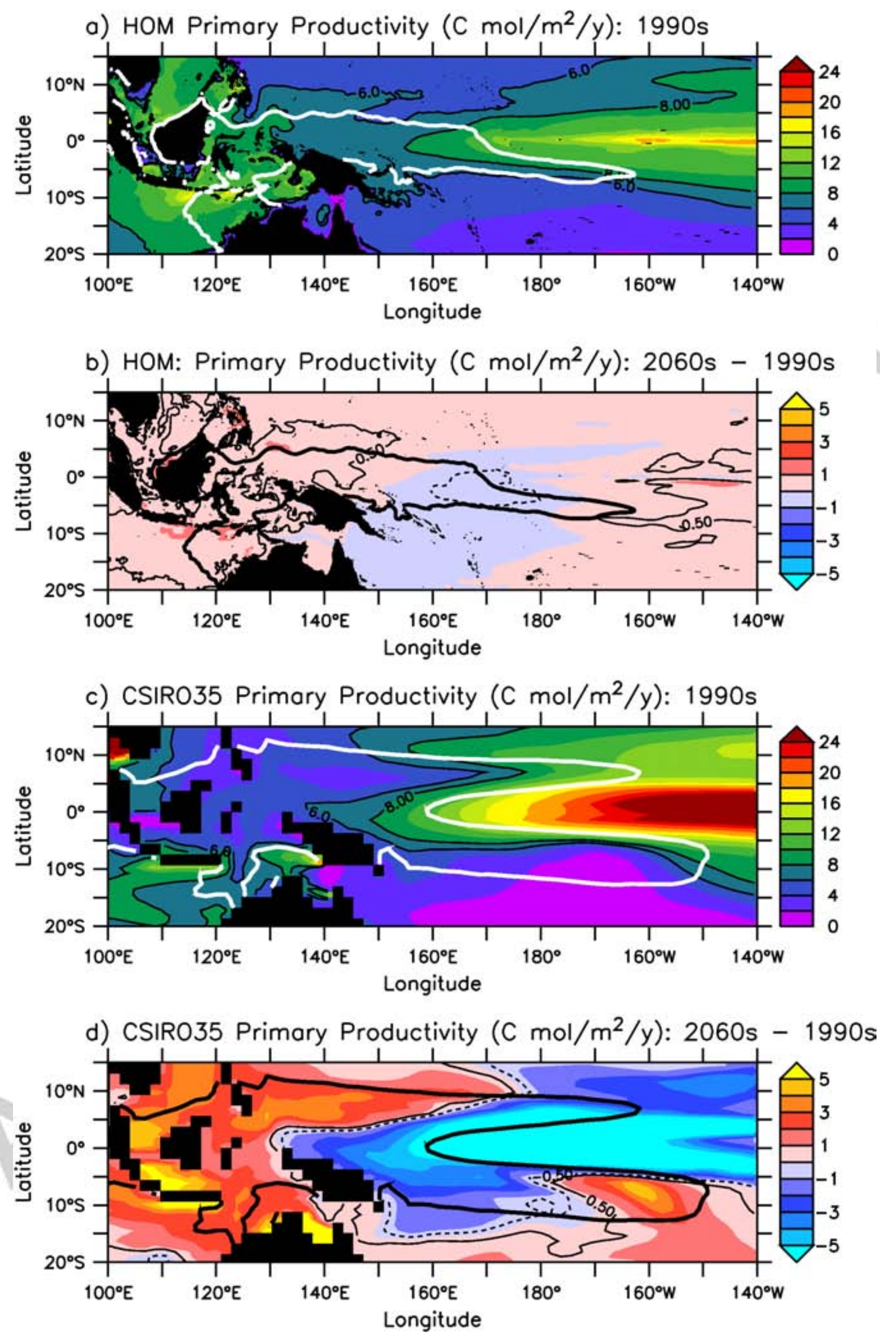

Figure 18: Simulated annual mean primary productivity (mol C/m^2/y): a) primary productivity from the 1990s HOM simulation; b) change in primary productivity between the 1990s and the 2060s obtained from the HOM projection; c) primary productivity from the 1990s CSIRO35 simulation; d) change in primary productivity between the 1990s and the 2060s obtained from the CSIRO35 projection. The thick black (white) lines represent the dynamic Warm Pool edge (Brown et al., 2013b) of the 1990s (2060s) in the respective simulations.

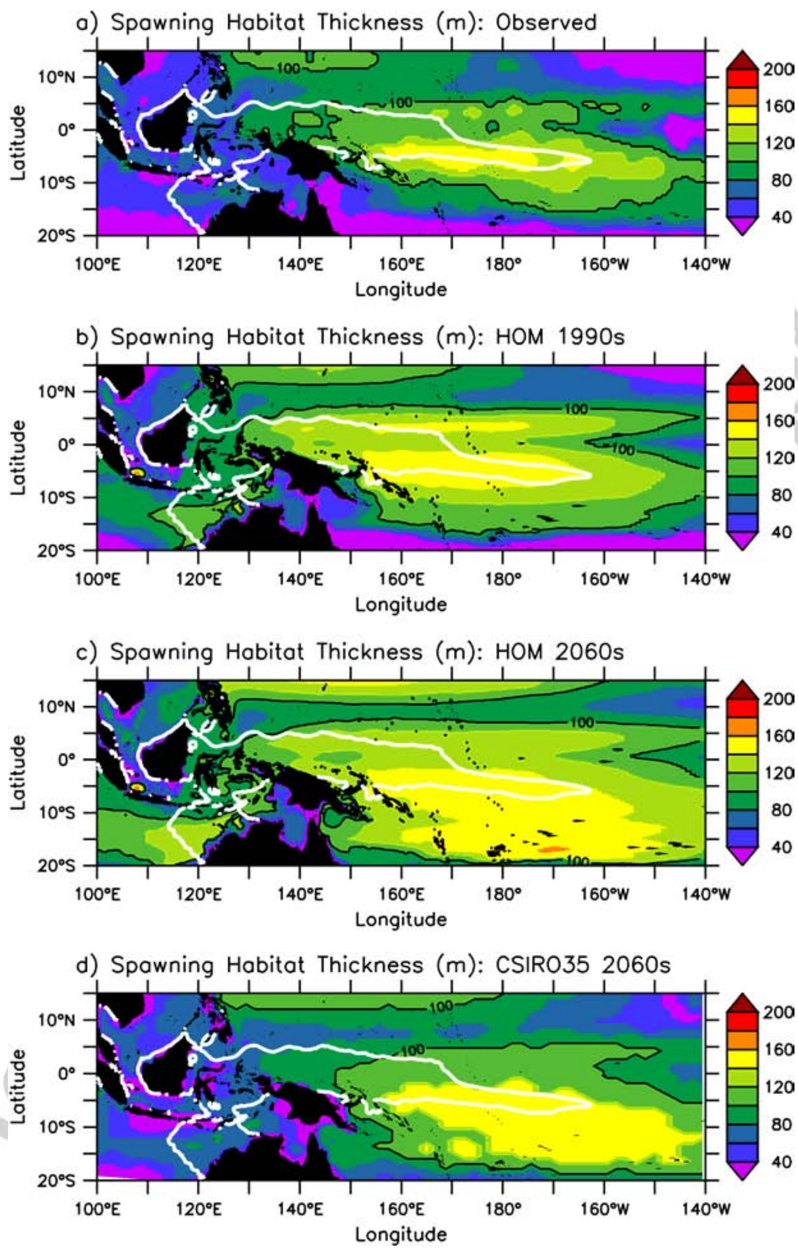

Figure 19: Suitable thermal habitat for spawning skipjack tuna, defined as the thickness of the water column with a temperature between 25°C and 32°C, from a) the observations based on CARS2009, b) the HOM simulation for the 1990s, c) the HOM simulation for the 2060s, and d) the bias-corrected CSIRO35 simulation for the 2060s. The thick white lines represent the dynamic Warm Pool edge (Brown et al., 2013b) in the 1990s HOM simulation.

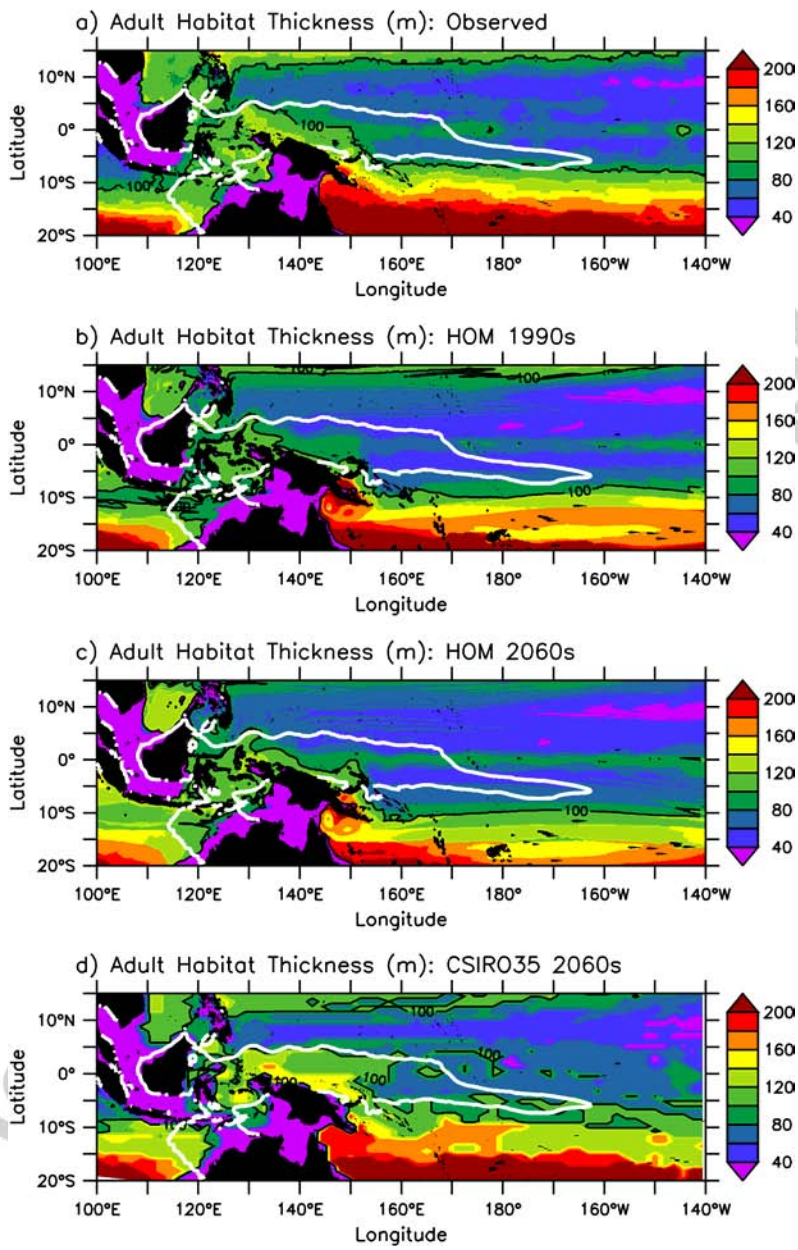

Figure 20: Suitable thermal habitat for adult skipjack tuna, defined as the thickness of the water column with a temperature between 20°C and 26°C, from a) the observations based on CARS2009, b) the HOM simulation for the 1990s, c) the HOM simulation for the 2060s, and d) the bias-corrected CSIRO35 simulation for the 2060s. The thick white lines represent the dynamic Warm Pool edge (Brown et al., 2013b) in the 1990s HOM simulation.

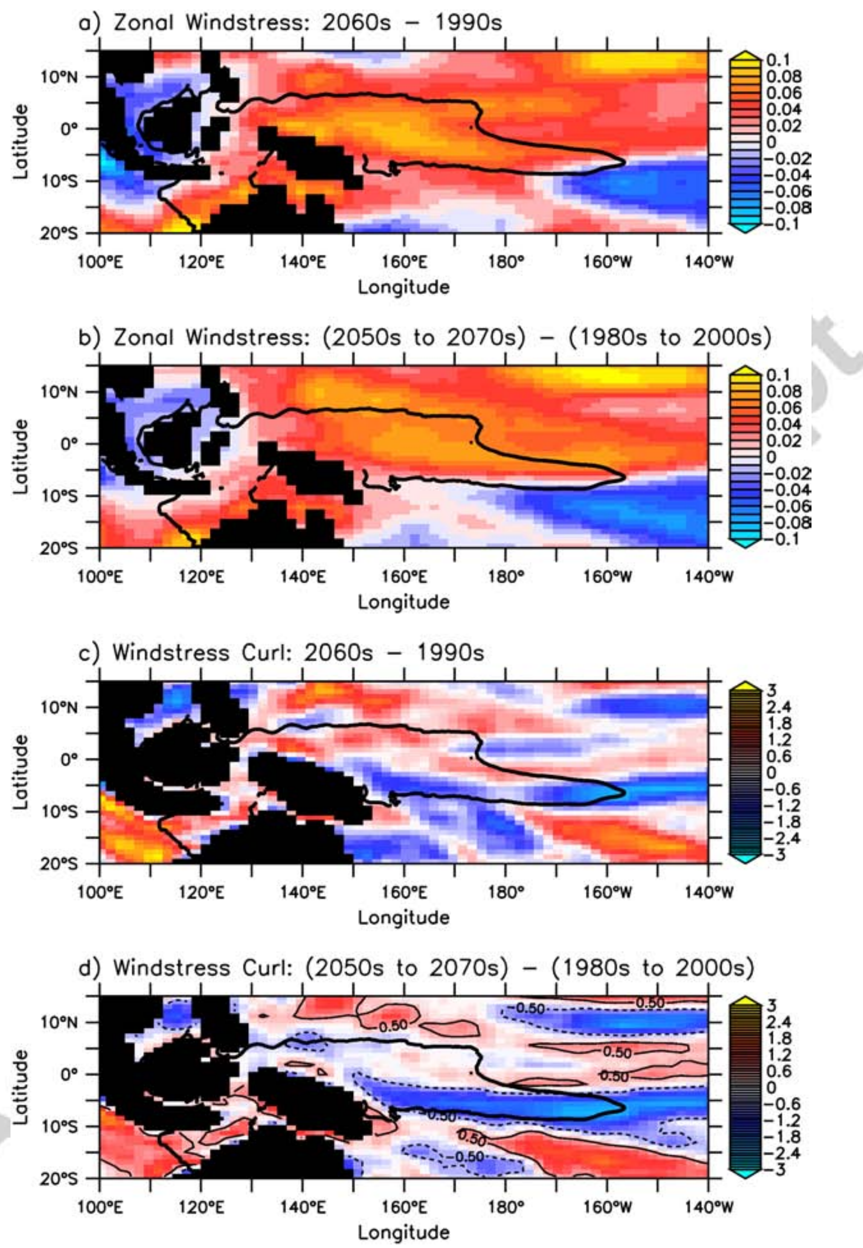

Figure 21: CSIRO35-simulated change in annual mean zonal windstress: a) between the 1990s and the 2060s; b) between 1980–2009 and 2050–2079. CSIRO35-simulated change in the annual mean windstress curl: c) between the 1990s and the 2060s; d) between 1980–2009 and 2050–2079. The thick black lines represent the dynamic Warm Pool edge (Brown et al., 2013b) in the 1990s HOM simulation.

Barber, R. T., Chavez, F. P., 1991. Regulation of primary productivity rate in the Equatorial Pacific. Liminology and Oceanography 36 (8), 1803–1815.

Behrenfeld, M. J., O'Malley, R. T., Siegel, D. A., McClain, C. R., Sarmiento, J. L., Feldman, G. C., Milligan, A. J., Falkowski, P. G., Letelier, R. M., Boss, E. S., 2006. Climate-driven trends in contemporary ocean productivity. Nature 444, 752–755.

Bell, J. D., Ganachaud, A., Gehrke, P. C., Griffiths, S. P., Hobday, A. J., Hoegh-Guldberg, O., Johnson, J. E., Le Borgne, R., Lehodey, P., Lough, J. M., Matear, R. J., Pickering, T. D., Pratchett, M. S., Gupta, A. S., Senina, I., Waycott, M., 2013. Mixed responses of tropical Pacific fisheries and aquaculture to climate change. Nature Climate Change 3 (6), 591–599.

Bosc, C., Delcroix, T., Maes, C., 2009. Barrier layer variability in the western Pacific warm pool from 2000 to 2007. Journal of Geophysical Research 114 (C6), C06023.

Brassington, G. B., Pugh, T., Spillman, C., Schulz, E., Beggs, H., Schiller, A., Oke, P. R., 2007. BLUElink development of operational oceanography and servicing in Australia. Journal of Research and Practice in Information Technology 39 (2), 151–164.

Brown, J. N., Gupta, A. S., Brown, J. R., Muir, L. C., Risbey, J. S., Whetton, P., Zhang, X., Ganachaud, A., Murphy, B., Wijffels, S. E., 2013a. Implications of CMIP3 model biases and uncertainties for climate projections in the western tropical Pacific. Climatic Change 119 (1), 147–161.

Brown, J. N., Langlais, C., Maes, C., 2013b. Zonal structure and variability of the Western Pacific dynamic warm pool edge in CMIP5. Climate Dynamics 19 September 2013, 1–16.

Chamberlain, M. A., Sun, C., Matear, R. J., Feng, M., Phipps, S. J., 2012. Downscaling the climate change for oceans around Australia. Geoscientific Model Development 5 (5), 1177–1194.

Christian, J., Verschell, M., Murtugudde, R., Busalacchi, A., McClain, C., 2002. Biogeochemical modelling of the tropical Pacific Ocean. II: Iron biogeochemistry. Deep-Sea Research Part II: Topical Studies in Oceanography 49, 545–565.

Collins, M., An, S.-I., Cai, W., Ganachaud, A., Guilyardi, E., Jin, F.-F., Jochum, M., Lengaigne, M., Power, S., Timmermann, A., Vecchi, G., Wittenberg, A., 2010. The impact of global warming on the tropical Pacific Ocean and El Niño. Nature Geoscience 3 (6), 391–397.

Condie, S. A., Dunn, J. R., 2006. Seasonal characteristics of the surface mixed layer in the Australasian region: implications for primary production regimes and biogeography. Marine and Freshwater Research 57, 569–590.

Cravatte, S., Delcroix, T., Zhang, D., McPhaden, M., Leloup, J., 2009. Observed freshening and warming of the western Pacific Warm Pool. Climate Dynamics 33 (4), 565–589.

Dietze, H., Matear, R., Moore, T., 2009. Nutrient supply to anticyclonic meso-scale eddies off western Australia estimated with artificial tracers released in a circulation model. Deep-Sea Research Part I: Oceanographic Research Papers 56 (9), 1440–1448.

DiNezio, P. N., Clement, A. C., Vecchi, G. A., Soden, B. J., Kirtman, B. P., Lee, S.-K., 2009. Climate response of the equatorial Pacific to global warming. Journal of Climate 22 (18), 4873–4892.

Dunn, J., Ridgway, K., 2002. Mapping ocean properties in regions of complex topography. Deep-Sea Research Part I: Oceanographic Research Papers 49, 591–604.

Durack, P. J., Wijffels, S. E., 2010. Fifty-year trends in global ocean salinities and their relationship to broad-scale warming. Journal of Climate 23 (16), 4342–4362.

Durack, P. J., Wijffels, S. E., Matear, R. J., 2012. Ocean salinities reveal strong global water cycle intensification during 1950 to 2000. Science 336 (6080), 455–458.

Ganachaud, A., Gupta, A. S., Brown, J. N., Evans, K., Maes, C., Muir, L. C., Graham, F. S., 2013. Projected changes in the tropical Pacific Ocean of importance to tuna fisheries. Climatic Change 119 (1), 163–179.

Han, W., Meehl, G. A., Hu, A., 2006. Interpretation of tropical thermocline cooling in the Indian and Pacific oceans during recent decades. Geophysical Research Letters 33 (23), L23615.

Johnson, G. C., Wijffels, S. E., 2011. Ocean density change contributions to sea level rise. Oceanography 24 (2), 112–121.

Kessler, W. S., Johnson, G. C., Moore, D. W., 2003. Sverdrup and nonlinear dynamics of the Pacific equatorial currents. Journal of Physical Oceanography 33 (5), 994–1008.

Kidston, M., Matear, R. J., Baird, M. E., 2011. Parameter optimisation of a marine ecosystem model at two contrasting stations in the Sub-Antarctic Zone. Deep-Sea Research Part II: Topical Studies in Oceanography 58, 2301–2315.

Large, W., Yeager, S. G., 2004. Diurnal to decadal global forcing for ocean and sea-ice models: The data sets and flux climatologies. Tech. Rep. NCAR/TN-460+STR, dOI: 10.5065/D6KK98Q6.

Le Borgne, R., Allain, V., Griffiths, S. P., Matear, R. J., McKinnon, A., Richardson, A. J., Young, J. W., 2011. Chapter 4: Vulnerability of open ocean food webs in the tropical Pacific to climate change. In: Bell, J. D., Hobday, A. J. (Eds.), Vulnerability of tropical Pacific fisheries and aquaculture to climate change. Secretariat of the Pacific Community, Noumea, New Caledonia.

Le Borgne, R., Barber, R. T., Delcroix, T., Inoue, H. Y., Mackey, D. J., Rodier, M., 2002. Pacific warm pool and divergence: temporal and zonal variations on the equator and their effects on the biological pump. Deep-Sea Research Part II: Topical Studies in Oceanography 49 (13), 2471–2512.

Lehodey, P., Bertignac, M., Hampton, J., Lewis, A., Picaut, J., 1997. El Niño Southern Oscillation and tuna in the western Pacific. Nature 389, 715–718.

Lehodey, P., Hampton, J., Brill, R. W., Nicol, S., Senina, I., Calmettes, B., Pörtner, H. O., Bopp, L., Ilyina, T., Bell, J. D., John, S., 2011. Chapter 8: Vulnerability of oceanic fisheries in the tropical Pacific to climate change. In: Bell, J. D., Hobday, A. J. (Eds.), Vulnerability of tropical Pacific fisheries and aquaculture to climate change. Secretariat of the Pacific Community, Noumea, New Caledonia.

Lehodey, P., Senina, I., Calmettes, B., Hampton, J., Nicol, S., 2013. Modelling the impact of climate change on Pacific skipjack tuna population and fisheries. Climatic Change 119 (1), 95–109.

Levitus, S., 2001. World Ocean Database, vol. 13. National Oceanic and Atmosphere Agency, US Department of Commerce.

Lukas, R., Lindstrom, E., 1991. The mixed layer of the western equatorial Pacific Ocean. Journal of Geophysical Research 96 (S01), 3343–3357.

Maes, C., 2008. On the ocean salinity stratification observed at the eastern edge of the equatorial Pacific warm pool. Journal of Geophysical Research 113 (C3), C03027.

Maes, C., Sudre, J., Garçon, V., 2010. Detection of the eastern edge of the equatorial Pacific warm pool using satellite-based ocean color observations. SOLA 6 (0), 129–132.

Matear, R. J., 1995. Parameter optimization and analysis of ecosystem models using simulated annealing: A case study at Station P. Journal of Marine Research 53, 571–607.

Matear, R. J., Chamberlain, M. A., Sun, C., Feng, M., 2013. Climate change projection of the Tasman Sea from an Eddy-resolving Ocean Model. Journal of Geophysical Research: Oceans 118 (6), 2961–2976.

McClain, C. R., Murtugudde, R., Signorini, S., 1999. A simulation of biological processes in the equatorial Pacific Warm Pool at 165°E. Journal of Geophysical Research: Oceans 104 (C8), 18305–18322.

Moore, T. M., Matear, R. J., Marra, J., Clementson, L., 2007. Phytoplankton variability off the Western Australian Coast: Mesoscale eddies and their role in cross-shelf exchange. Deep-Sea Research Part II: Topical Studies in Oceanography 54, 943–960.

Nakicenovic, N., Alcamo, J., Davis, G., de Vries, B., Fenhann, J., Gaffin, S., Gregory, K., Grubler, A., Jung, T. Y., Kram, T., Lebre La Rovere, E., Michaelis, L., Mori, S., Morita, T., Pepper, W., Pitcher, H., Price, L., Riahi, K., Roehrl, A., Rogner, H. H., Sankovski, A., Schlesinger, M., Shukla, P., Smith, S., Swart, R., van Rooijen, S., Victor, N., Dadi, Z.,

2000. IPCC Special Report on Emissions Scenarios (SRES). Cambridge University Press, UK.

Oke, P. R., Brassington, G. B., Griffin, D. A., Schiller, A., 2008. The Bluelink ocean data assimilation system (BODAS). Ocean Modelling 21 (1-2), 46–70.

Picaut, J., Ioualalen, M., Menkes, C., Delcroix, T., McPhaden, M. J., 1996. Mechanism of the zonal displacements of the Pacific Warm Pool: Implications for ENSO. Science 274 (5292), 1486–1489.

Reynolds, R. W., Smith, T. M., 1994. Improved global sea surface temperature analyses using optimal interpolation. Journal of Climate 7, 929–948.

Ridgway, K., Dunn, J., Wilkin, J., 2002. Ocean interpolation by four-dimensional weighted least squares—application to the waters around Australasia. Journal of Atmospheric and Oceanic Technology 19, 1357–1375.

Rotstayn, L. D., Collier, M. A., Dix, M. R., Feng, Y., O'Farrell, S. P., Smith, I. N., Syktus, J., 2010. Improved simulation of Australian climate and ENSO-related rainfall variability in a global climate model with an interactive aerosol treatment. International Journal of Climatology 30, 1067–1088.

Ryan, J. P., Polito, P. S., Strutton, P. G., Chavez, F. P., 2002. Unusual large-scale phytoplankton blooms in the equatorial Pacific. Progress in Oceanography 55 (3-4), 263–285.

Sen Gupta, A., Ganachaud, A., McGregor, S., Brown, J. N., Muir, L., 2012. Drivers of the projected changes to the Pacific Ocean equatorial circulation. Geophysical Research Letters 39 (9), L09605.

Steinacher, M., Joos, F., Frölicher, T. L., Bopp, L., Cadule, P., Cocco, V., Doney, S. C., Gehlen, M., Lindsay, K., Moore, J. K., Schneider, B., Segschneider, J., 2010. Projected 21st century decrease in marine productivity: a multi-model analysis. Biogeosciences 7 (3), 979–1005.

Sun, C., Feng, M., Matear, R. J., Chamberlain, M. A., Craig, P., Ridgway, K. R., Schiller, A., 2012. Marine downscaling of a future climate scenario for Australian boundary currents. Journal of Climate 25 (8), 2947–2962.

Taylor, A. H., Geider, R. J., Gilbert, F. J. H., 1997. Seasonal and latitudinal dependencies of phytoplankton carbon-to-chlorophyll *a* ratios: results of a modelling study. Marine Ecology Progress Series 152 (1-3), 51–66.

Uppala, S. M., Kallberg, P. W., Simmons, A. J., Andrae, U., Bechtold, V. D., Fiorino, M., Gibson, J. K., Haseler, J., Hernandez, A., Kelly, G. A., Li, X., Onogi, K., Saarinen, S., Sokka, N., Allan, R. P., Andersson, E., Arpe, K., Balmaseda, M. A., Beljaars, A., Van De Berg, L., Bidlot, J., Bormann, N., Caires, S., Chevallier, F., Dethof, A., Dragosavac, M., Fisher, M., Fuentes, M., Hagemann, S., Holm, E., Hoskins, B. J., Isaksen, L., Janssen, P., Jenne, R., McNally, A. P., Mahfouf, J. F., Morcrette, J. J., Rayner, N. A., Saunders, R. W., Simon, P., Sterl, A., Trenberth, K. E., Untch, A., Vasiljevic, D., Viterbo, P., Woollen, J., 2005. The ERA-40 re-analysis. Quarterly Journal of the Royal Meteorological Society 131 (612), 2961–3012.